Optimizing Sensitivity of Capacitive Pressure Sensors for Improved Intraocular Pressure Monitoring

Exploring the Impact of Spiral Shaped Antenna Geometries on Q-Factor and Resonance Frequency Output

by

Kiana Isabella Griffith

to obtain the degree of Master of Science in Biomedical Engineering
at the Delft University of Technology.

Student number:	5471680	
Project duration:	March, 2023 – August, 2023	
Thesis committee:	Dr. D. G. Muratore,	TU Delft, Supervisor
	Dr. C. Boutry,	TU Delft, Supervisor

TU Delft

Dedication

First and foremost, this thesis is dedicated to my parents and sister, who have offered unconditional support, love, and motivation from the other side of the world. During times when I couldn't find encouragement within myself, you were there, lifting me up with your belief in me. I cannot express enough gratitude for having such an unconditional support system. I cherish the love and inspiration you have showered upon me. Also, to my closest friends who have impacted me in so many ways over the last few years, I am so grateful to you. Bridget, I am eternally grateful for being placed in a church with no heating for lectures that brought us together. I am so proud of how our lives have progressed over the last few years and cannot wait to see where we both end up. Larissa, coming home to you over the last 2 years brightened up every day, I will miss you.

I am also incredibly grateful to the wonderful friends and colleagues who surrounded me during my time in Delft. Not only did you all offer invaluable technical support (CST tutors!), but also provided emotional strength knowing we were all navigating the same challenging situations. Your unwavering camaraderie has made the last two years all the more enriching and unforgettable. Especially you Samhitha, every coffee and hot-chocolate break made each day more bearable! Side-note dedication to Engineering tutorial center on Youtube for helping me navigate CST Studio Suite.

Additionally, Grandma, this thesis is dedicated to you. Whilst you may not be here to witness my graduation, you were there to watch me start my master's degree. Your pride in me is incomparable, your belief in my abilities has shaped me into the person I am today and I carry your love with me as I reach this milestone. I dedicate this achievement to you with all my love.

Acknowledgements

Without the encouragement, guidance, and supervision of Dr. Dante Muratore and Dr. Clementine Boutry, this project would not have been possible. The opportunity to work on such a multi-disciplinary project has been a challenging, eye-opening experience. Additionally, I am grateful for their ready availability to meet whenever needed, which significantly enriched the entire experience. Their belief in this work and their dedication to helping me succeed have left a lasting impact that I will forever cherish.

I extend my sincere gratitude to Dr. Wishal Ramdas from Erasmus MC for his invaluable insights into the clinical necessities driving the device's development. His guidance highlighted unexplored challenges faced by clinicians, both in the operating room and post-operative phases, refining the study.

I also appreciate Floris Idema and Paolo Soleri for their collaborative spirit, enthusiasm, and insightful perspectives. Their expertise in device development and business aspects has not only guided the current project but has also ignited innovative thinking for future endeavors.

Kiana Griffith
Delft, August 2023

***Abstract*—This thesis analyzes and describes a wearable pressure sensor to detect intraocular pressure and guide clinician diagnosis of glaucoma. Although glaucoma has many symptoms and risk factors, high intraocular pressure is the most predominant. A method to continuously and accurately record intraocular pressure measurements and fluctuations in a patient could lead to a more reliable glaucoma diagnosis and a better understanding of glaucoma progression. The proposed sensor consists of an ecoflex dielectric layer, between two graphene-silver nanowire spiral antenna electrodes which also act as the membrane structure. The sensor deflection depends on the intraocular pressure fluctuations; higher pressure leads to larger deflection values, therefore, larger capacitance change. The capacitance change leads to a shift of the resonant frequency, which is simulated in this thesis. The sensor must be smaller than 11 mm^2 to fit on a commercial lens. Specifically, this thesis analyzes and simulates the effects of electrode thickness and shape on the overall performance of the sensor. The optimum geometry of the capacitive sensor is analyzed to maximize sensor sensitivity and quality factor, with a correlated frequency appropriate for a wearable lens. Using Computer Simulation Technology, the optimized antenna dimensions are spiral-electrodes with a plate thickness of 350μm, and 3 spiral revolutions; leading to an increase in sensitivity of 1.4 MHz/mmHg.**

***Index Terms*—Intraocular Pressure, Wearable Contact Lens Sensor, Graphene-Silver-Nanowire, Spiral Antenna**

I. Introduction

Glaucoma is a neurodegenerative disorder characterized by the slow impairment of vision and is the second leading cause of blindness worldwide. It requires continuous monitoring and treatment of intraocular pressure (IOP) fluctuations to impede disease progression [1]. It is often asymptomatic until the later stages, when peripheral vision becomes slightly blurred. Unfortunately, glaucoma is typically diagnosed only after significant damage to the optic nerve has occurred, making it irreversible. An increase in IOP leads to compression of the lamina cribrosa, a porous structure located at the back of the eye (Fig. 1), resulting in impaired retinal ganglion axons and subsequent damage to the optic nerve [2]. This rise in IOP is attributed to a disturbance in the equilibrium between the production of aqueous humor and its drainage through the trabecular meshwork [3]. The iris ciliary body in the posterior chamber of the front eye produces aqueous humor, which accumulates in the posterior chamber and then flows through the pupil into the anterior chamber. From the anterior chamber, the aqueous humor drains through three different pathways: 1. The aqueous humor mostly drains through the trabecular meshwork at the angle of the anterior chamber and enters the Schlemm canal, eventually reaching episcleral veins; 2. Some of the aqueous humor flows into the suprachoroidal space and enters the venous circulation which is in the ciliary body, sclera, and the choroid; 3. A minor amount of aqueous humor passes through the iris and returns to the posterior chamber [4].

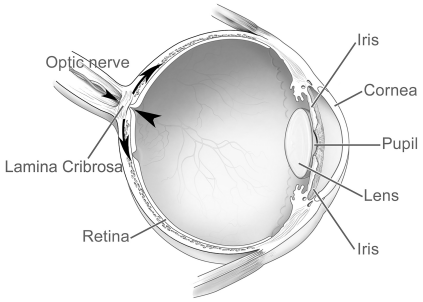

Fig. 1. Anatomical schematic of the eye [5].

The current methods for measuring IOP lack consideration for various external factors such as diet, exercise, sleep, amongst others; thus impeding the development of an ideal device for accurate IOP assessment [6]. Moreover, its dynamic diurnal nature is influenced by several internal factors, including posture, blood pressure, corneal thickness, stress, and the time of measurement [7]–[9]. Neglecting these factors can result in the under- or over-estimation of IOP levels, leading to delayed diagnoses and an increased risk of blindness for patients [10].

In a healthy individual, IOP ranges between 10-21 mmHg (millimeters of mercury) [1], whereas glaucomatous patients exhibit elevated IOP above 30 mmHg and experience larger fluctuations. The current gold-standard method for measuring IOP is Goldmann applanation tonometry (GAT), which assesses force required to deform the cornea over a set area. However, GAT measurements are limited to clinical settings and may not provide a comprehensive representation of a patient's actual IOP due to diurnal variations, environmental influences, and intrinsic factors mentioned above [11], [12]. Moreover, GAT readings can be influenced by individual variations in corneal thickness and rigidity, potentially leading to overestimation of IOP [12]. Several factors contribute to glaucoma risk, but IOP remains the only modifiable parameter. Therefore, continuous monitoring and management of IOP fluctuations are crucial in preventing the progression of glaucoma. As an alternative, the development of a device capable of continuously recording IOP would overcome present issues, enabling the detection of fluctuations and facilitating timely intervention to impede glaucoma progression. Additionally, such a device would offer improved usability and comfort for wearers, reducing the need for invasive surgical procedures.

Recent advancements have led to the development of medical electronic devices for continuous monitoring of IOP in patients [13]–[23]. Devices based on various principles have been proposed and can be widely divided into implantable and wearable devices. Implantable sensors require surgical procedures where pressure-sensitive elements are placed in the eye, limiting their clinical applicability due to the associated damage [24], [25].

[1]Pressure SI unit is Pascals, for IOP sensing devices mmHg is used where 1 mmHg = 0.13332 kPa.

Implantable active lenses present extreme challenges due to the limited population requiring invasive surgery. Surgery for monitoring IOP is undesirable and should be prevented where possible. Non-invasive IOP sensors can be further classified as optical or electrical. Electrical IOP sensors include capacitive, inductive, and piezo-resistive types. Capacitive and inductive sensors, although achieving higher sensitivities and responsivities (e.g. Responsivity of 8 kHz/mmHg in [16]) requires additional equipment for signal reading, hindering portability and continuous monitoring [16]. Resistance strain sensors provide miniaturization potential but have lower sensitivity (e.g., 113 μV/mmHg by [26] [2].). Capacitive pressure sensors (CPS) are highly favored for their fast response, reversibility, temperature insensitivity, simple structure, ease of fabrication, and low energy consumption. However, their sensitivity is often constrained by the modest changes in capacitance observed in parallel plate configurations [27]. Improving sensor sensitivity can enhance measurement precision and disturbance resistance, and reduce the need for high-precision reading devices, thereby reducing costs.

Recent advancements in LC-resonant-based IOP sensing devices have progressed significantly due to their convenience, ability to monitor IOP over a 24-hour period, and potential for wide clinical population implementation. A wearable IOP device using an LC-resonant circuit does not require surgery or complex, expensive, battery-powered chips, thus eliminating the need for an implantable battery. However, wireless passive LC-resonant IOP sensing devices require close contact with an external read-out to ensure efficient data transfer.

The work in [17] proposed a capacitive contact lens sensor for continuous and non-invasive IOP monitoring, capable of accurately tracking pressure variations over time [17]. The sensor demonstrated an IOP sensitivity of up to 23.8 kHz/mmHg [3]The authors proceeded to alter the device to improve the sensitivity discussed in [16]. A piezoresistive-based wearable sensor using strain gauges fabricated with Gr-NW achieved a sensitivity of 42250 ppm/mmHg [4] [28]. The device presented in [29] was developed using a platinum (Pt) strain gauge fabricated through Micro-electromechanical systems (MEMS) process, which achieves a sensitivity of 289.5 μV/mmHg [29]. Another wireless passive contact lens sensor (CLS), uses a capacitive sensor, which correlates the curvature of the lens with the resonance frequency of the sensor to determine IOP. The device used a stretchable coil and a micro-fabricated capacitor made of gold and titanium thin films sandwiched between multi-layer parylene-C. The sensor exhibited a sensitivity of 35.1 kHz/mmHg, although being the responsivity of the sensor, it represents the sensor sensitivity per mmHg of change in the eye [18]. Whilst offering high sensitivity and efficient recording, these devices do not address feedback from patient trials which typically desire more flexible and transparent materials for increased user comfort. The device proposed in [13] developed a graphene silver-nanowire (Gr-AgNW) capacitive IOP sensor integrated into a contact lens that monitors IOP changes in real-time by detecting lens deformation on the cornea based on an LC-resonance circuit [13]. The sensor's high transparency and conductivity is facilitated by the Gr-AgNW material, and it reaches a sensitivity of 2.2 MHz/mmHg. Further research on this sensor may advance wearable IOP monitoring and enhance glaucoma management. Table I compares existing wearable IOP sensing devices which utilize inductive coupled telemetry-based systems. An overview table of IOP sensing devices can be seen in Appendix VI-A.

TABLE I
Comparison of wearable IOP sensing devices.

Reference	Ideal sensor	[13] This device	\[17]	\[16]	\[19]	\[18]
Drift	None	-	n/a	n/a	n/a	n/a
Pressure accuracy	<1 mmHg	2.2 mmHg	200 ppm/mmHg	n/a	n/a	n/a
Resonant frequency	4 GHz	4.1 GHz	119 MHz	215 MHz	551 MHz	490 MHz
Detectable range (mmHg)	0 - 50	5 - 50	5 - 40	5 - 40	0 - 50	0 - 55
Sensitivity (frequency response)	<30 kHz/mmHg	2.2 MHz/mmHg	23 kHz/mmHg	8 kHz/mmHg	57 kHz/mmHg	35.1 kHz/mmHg

This thesis focuses on a CPS designed with two spiral antennas surrounding a dielectric layer, forming an LC-resonance circuit for wireless data transfer. Geometric considerations are investigated to optimize its performance, including increased resonant frequency responses at various pressures and achieving a high Q-factor for efficient energy transfer. These optimizations aim to enhance the sensitivity and efficiency of the sensor for improved continuous IOP monitoring. Section II displays the initial sensor design and sensing method of the device. Section III discusses the methodology of the project, the modeling and simulation environments, and the measurements required to improve device sensitivity. Section IV presents the result outcomes. Section V analyzes the findings, discusses implications, and presents an outlook for future work on this sensor.

II. Sensor Design

Typically, IOP exhibits fluctuations of approximately 4-6 mmHg during the day, increasing to 15 mmHg in glaucoma patients [30]. Therefore, the device's pressure resolution and range play a vital role in aiding glaucoma diagnosis. It is essential for the device to accurately record IOP within this range, with a minimum required resolution of 2 mmHg for clinical purposes [31]. All required parameters are summarized in Table II.

[2]Capacitive and inductive sensors will have a sensitivity output in kHz/mmHg, whereas resistance strains sensors report the sensitivity in V/mmHg

[3]Sensitivity in kHz/mmHg is calculated from the original ppm/mmHg measurement, the resonance frequency must be known. Frequency change = ppm * f_0/1000000.

[4]The resonant frequency is not known, and therefore cannot be converted to kHz/mmHg.

TABLE II
Technical requirements of a wearable IOP sensing device.

Parameter	Value
Detectable pressure range	0-50 mmHg
Pressure resolution	2 mmHg
Continuous monitoring	24 hour minimum
Dimensions	Maximum diameter of 11 mm
Thickness	Maximum thickness of 1mm

To detect IOP fluctuations on the mmHg scale, accurately translating ocular volume changes to corresponding pressure changes in mmHg is required. IOP changes the corneal curvature radius by exerting mechanical force on the cornea. Higher IOP leads to corneal steepening, causing a decrease in curvature radius, while lower IOP may result in corneal flattening or a larger curvature radius [32]. To achieve high sensitivity, various factors must be taken into account during the design of the sensing device.

In this thesis, the sensing device proposed in [13] is adapted to improve the sensitivity. The sensor originally consists of two spiral antennas, respectively 500um and 120um thick fabricated using a Gr-AgNW hybrid material, placed above and below a dielectric Ecoflex 00:30 sensing layer. The spiral antennas form the plates of a capacitive IOP sensor, while the top spiral (500um thickness) is responsible for coupling to an external antenna for wireless read-out. Multi-turn spiral is utilized as the inductive coil of the device, and it is designed to reach a high q-factor for maximum resolution of the LC resonant circuit. An increase in IOP causes deflection of the device, leading to capacitance and inductance increase by expansion of the inductor coils, which causes the resonance frequency to shift. The sensing component of the device can be seen in Figure 2.

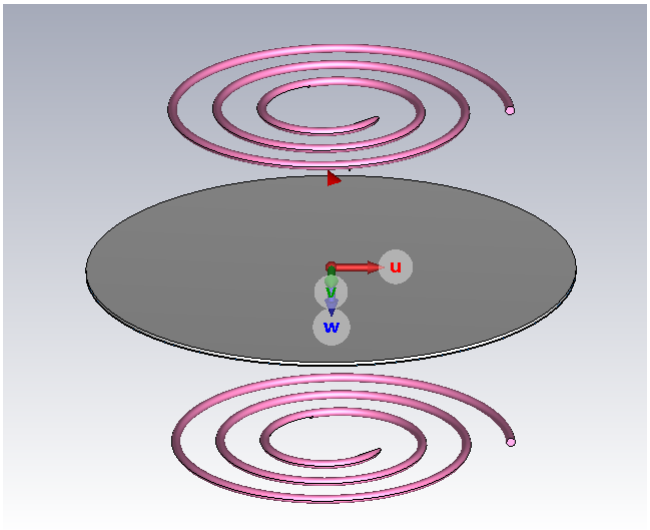

Fig. 2. Sensing device based on model from [13].

The device proposed in [13] demonstrates the potential for simultaneous monitoring and diagnosis of glaucoma and diabetes, which commonly coexist [33]. The CLS utilizes Ecoflex as the compressible dielectric layer and Gr-AgNw electrodes, offering flexibility and transparency. This configuration enables detection of IOP fluctuations by measuring capacitance variations resulting from the compression and deflection of the Ecoflex layer. The device also incorporates controlled amounts of Gr-AgNW in the dielectric layers to optimize a field-effect transistor (FET) sensor's performance in detecting IOP variations and glucose levels [13]; however, in this thesis, the glucose-sensing FET sensor is neglected to focus on improving the sensitivity of IOP detection. The device offers a pressure resolution of 2.2 mmHg, detects IOP fluctuations in the range of 5-50 mmHg, has 90% optical transmittance, and operates at a frequency of 4.1 GHz [13]. The whole device should fit on a standard commercial lens, and therefore be less than $11mm^2$ in diameter when considering the device encapsulation as well; the full technical specifications of the device are presented in Table III.

TABLE III
Properties of device presented in [13].

Sensor properties	Value
Sensitivity (with FET Sensor)	0.00162 kPa
Detectable pressure range	5-50 mmHg
Pressure resolution	2.2 mmHg
Operational frequency	4.1 GHz

The capacitance (C) change can be expressed as a function of the distance between the plates (proportional to the deflection of the sensor) by [34]:

$$C = \frac{e_0 e_r A}{d}$$

- ϵ_0 = permittivity of free space
- ϵ_r = relative permittivity of the dielectric material (related to its ability to store an electric field)
- A = plate area.
- d = distance between the plates.

By optimizing these parameters, the sensor's sensitivity to pressure changes can be enhanced. These changes can ultimately be made through variations in the spirals and their corresponding thickness.

A. *Device Fabrication*

Material selection for IOP wearable sensors is not yet standardized, given the novelty of this technology. In the context of biomedical CPSs, a common configuration involves placing a dielectric conductive layer between two inductive plates. In this work, Ecoflex is used as the dielectric layer and Gr-AgNW for the plates. The use of inductive materials for the plates establishes an LC circuit to facilitate wireless data transfer.

The device was fabricated following the procedure below [13]:

1) Silver Nanowire films: AgNWs with a diameter of 30 nm and length of 25 mm dispersed in deionized water. The dispersion was spin-coated on a target substrate for 30s at 500 r.p.m. to get the lowest sheet resistance. The substrate was then annealed at 150 C for 90 s to completely evaporate the water.
2) Chemical vapor deposition (CVD) of graphene: Copper foil cleaned and loaded into the CVD chamber. Graphene synthesis carried out, and chamber is cooled to room temperature with Argon flowing. To transfer the synthesized graphene onto a target substrate, Polymethyl methacrylate (PMMA) was spin-coated on the graphene-on-Cu foil. To remove the foil it is floated on a diluted etchant, which leaves a PMMA-coated layer. The graphene-PMMA was rinsed with deionized water, and the layer was transferred onto a substrate, followed by removal of PMMA by acetone.
3) IOP Sensor Fabrication: Copper foil coated with parylene. Silver nanowrie suspension spin-coated and annealed onto parylene substrate, and spiral coil is patterned by conventional etch-back process using photoresist and reactive ion etching (RIE). Ecoflex 00-30 then spin coated above the bottom silver nanowire spiral. After, top silver nanowire spiral formed by same method as bottom coil, foiled by passivation of device by another parylene layer. The bottom copper foiled etched by nickel etchant, device transferred onto contact lens. Central area then punched to allow permeation of oxygen and water

B. Wireless Sensing Method

An antenna converts electric currents into electromagnetic waves and conversely. It exhibits varying reactances at different frequencies. When the magnitudes of the inductive and capacitive reactances become equal and cancel each other out at a specific frequency, the antenna becomes resonant, and its impedance becomes purely resistive [35].

The passive sensor employed operates on the principles of an LC circuit. This LC passive sensor is comprised of two fundamental components: the pressure-dependent variable capacitor, serving as the core sensing element, and an inductor that functions as the antenna (spiral antenna in this case), forming an LC circuit. The resonant frequency of the sensor varies with applied pressure, enabling wireless data transfer. To achieve wireless communication, an external antenna is utilized for readout.

Wireless sensing offers several advantages, including portability and enhanced user comfort by eliminating the need for wired connections. For successful implementation, selecting an appropriate operating frequency is critical to minimize energy absorption by surrounding tissue and achieve an optimal sensing distance. This intentional design aims to attain high sensitivity and Q-factor, making the sensor suitable for inductively coupled wireless IOP monitoring.

For efficient wireless communication, the antenna coils are made using Gr-AgNW due to its advantageous combination of optical transparency and electrical conductivity. In initial testing in [13] a reader antenna inductively couples and powers the remote sensor at a distance of 10mm. The resistance change of the graphene induces a shift in the resonant frequency. The resonance frequency shifts in response to pressure can be detected through an inductive telemetry link utilizing an external readout antenna. The readout device excites the sensor's circuit, supplying an impedance load that reflects onto the external antenna. The resonance frequency is represented by the following equation:

$$f_0 = \frac{1}{2\pi}\frac{1}{\sqrt{L_s C_s}}$$

if

$$R_s^2 << \frac{L_s}{C_s}$$

- L_s represents the sensor inductance
- C_s represents the sensor capacitance
- R_s represents the sensor resistance

The device circuit is illustrated in Figure 3, illustrating a resonant circuit comprising an inductor (L_{sensor}) and a capacitor (C_{sensor}). This sensing circuit is inductively coupled to the external reader circuit on the left. The readout circuit consists of an inductor (L_{read}) and a resistor (R_{read}), representing the readout coil resistance, which is equivalent to the sensor's resistance (R_{sensor}).

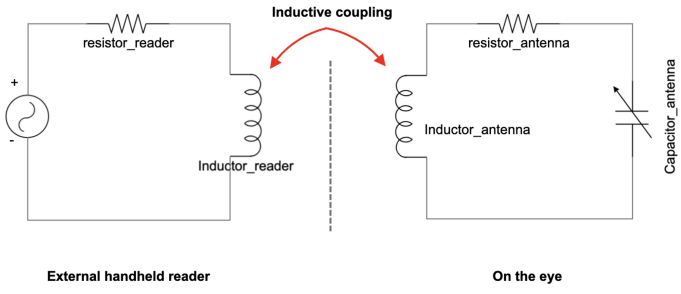

Fig. 3. Schematic of the LC circuit representing the IOP sensing device and reader.

C. Sensor performance parameters

The resonance frequency of the sensor refers to the frequency at which the sensor's capacitive and inductive components resonate, leading to maximum energy transfer. By simulating these shifts, the capacitance changes as the sensor expands or contracts under varying pressure

conditions can be shown. The second parameter, the Q-factor, is a dimensionless parameter which characterizes the sharpness or selectivity of the resonance in the sensor's LC circuit. A high Q-factor indicates efficient energy transfer around the resonant frequency, enabling accurate detection of small capacitance changes and high sensitivity [36]. However, an extremely high Q-factor may lead to practical challenges, such as increased noise susceptibility and sensitivity to environmental variations, potentially reducing system robustness [36]. Conversely, a low Q-factor results in a broader resonance peak, compromising sensitivity and accuracy in pressure measurements; while it may provide better noise immunity and robustness, it compromises the sensor's ability to detect small changes in capacitance accurately cite [36]. Striking a balance within a suitable Q-factor range is essential for optimizing the sensor's performance. The optimal Q factor may vary based on specific design parameters, necessitating a thorough evaluation.

III. Methodology, Modeling and Geometric Optimization

To simulate and analyze the behavior of the proposed CPS, COMSOL Multiphysics and Computer Simulation Technology Studio Suite (CST) is used. Key parameters, including material properties, dimensions, and excitation conditions are considered in the simulations to ensure accuracy and relevance. A basic overview of the two-step methodology can be seen in Figure 4. The analysis evaluates the sensor's Q-factor and resonance frequency shift, which are critical outputs in determining the sensor's sensitivity and efficiency. Through this methodology, valuable insights into the behavior of the CPS can be understood, contributing to its optimization and viability for wearable lens-based IOP monitoring applications. A GitHub repository has been created to store the design of all models created, as well as the Q-factor data and ASCII data for resonance frequency plots (repository available upon request). Additionally, Appendix VI-G contains the design overview for visual understanding of the designs, along with the associated resonance frequency plots.

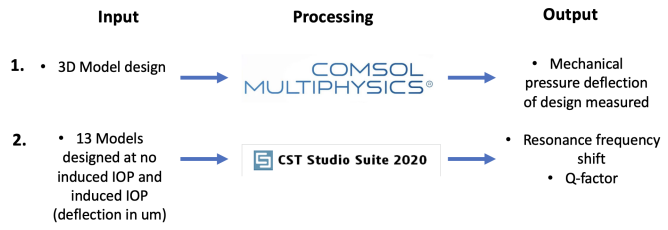

Fig. 4. Methodology figure.

A. Modeling and Simulation Setup

The thickness of the spiral electrodes as well as the revolutions of the spiral were the parameters swept to determine the maximum possible coupling between the sensor itself and the antenna. Figure 5 displays a perspective view of the original design modelled in CST.

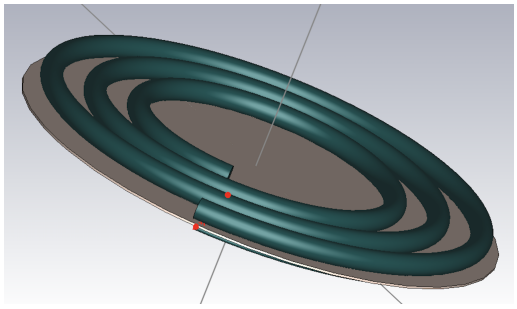

Fig. 5. Original design from [13] modelled in CST.

Model Design

The CPS was initially simulated using COMSOL to measure the deflection of the structure. The methodology of the initial design is explained below. The same steps were followed to produce designs of varying thicknesses and spiral turns.

- Initial geometry defined
- Material properties defined: Each component is assigned individual material properties. The base material of Silicone and silver was used and then adjusted to represent Ecoflex and Gr-AgNw.
- Component definition: defined the spirals as the electrodes, defined the Ecoflex layer as the dielectric, and encased the device in a cylinder to represent the device functioning in air.
- Mesh: Generated a tetrahedral mesh which captured full details of the dielectric layer and spiral antenna.
- Defined boundary conditions: The voltage assigned on the top spiral antenna and bottom spiral antenna grounded. Therefore, altering the capacitance when deflection is induced.
- Pressure load: Pressure induced from the bottom to the top spiral antenna to simulate increase in IOP. The pressure simulated ranged from 0-8000 Pa to represent an IOP change of 0-60 mmHg.
- Solver settings: Transient analysis simulated to measure the pressure change. Deflection induced plots created, as well as capacitance change simulated.

The materials used in the device are Ecoflex and Gr-AgNW for the dielectric layer and spiral antennas, respectively. These materials do not exist on the material libraries in COMSOL or CST; therefore, parameters must be manually input. The values are seen in Table IV.

TABLE IV
Material properties utilized in this project.

Material	Dielectric constant	Youngs modulus	Conductivity	Density
Gr-AgNW [37]	113 [3]	160 GPa	6x10$^5 S/m$	-
Ecoflex 00-30 [38]	2.17	0.125 MPa	0.16 W mK1	0.40
Graphene [39]	6.9	1 Tpa	80×10$^6 S/m$	2.27
AgNw [40], [41]	-	83 GPa	6.3×10$^7 S/m$	0.785

COMSOL Multiphysics Simulations

Whilst COMSOL Multiphysics is a versatile platform, it is not optimized to be used in high-frequency EM simulations. It has limited features with respect to S-parameter analysis and frequency-solvers; it can hinder accurate simulations of the designed CPS. Therefore CST was used for EM simulations. COMSOL Multiphysics was used solely to demonstrate physical deflection induced by mechanical pressure, as CST does not allow for physical deflection induced by pressure. In addition, CST was used because of the limitations in specialized features when designing the models themselves; for example, designing the spiral coil antenna in COMSOL requires the following steps:

1) Use the component builder to define the spiral
2) Create a polygon for the spiral
3) Draw the cross-section of the antenna spiral by clicking on the circumference of the wire spiral radius to form a polygon. Repeat this four times to form the antenna spiral, which will have a rectangular cross-section
4) Revolve the component around the axis to form the 3D spiral shape
5) Adjust the parameters to have a set number of turns and diameter

In comparison, CST Studio Suite allows a 3D model spiral to be directly selected from a component library, and adjusted depending on individual needs. This further justifies the decision to use CST Studio Suite to design all models, as 13 different models were designed.

The original design dimensions can be seen in Table V below.

TABLE V
Table with original sensor dimensions.

Parameter	Value
Diameter Ecoflex	11 mm
Diameter maximum spiral	11 mm
Thickness Ecoflex	50 um
Diameter spiral antenna top	500 um
Diameter spiral antenna bottom	120 um

CST Studio Suite Simulations

CST was used for analysis of resonance frequency shifts in response to variations in spiral antenna thickness and the number of turns, providing insights into how capacitance changes as the sensor undergoes expansion or contraction due to applied pressure. Additionally, CST is used to analyze the sensor's Q-factor in relation to spiral antenna dimensions. By observing Q-factor variations, the energy transfer efficiency is assessed. Fine-tuning the sensor characteristics ensures the desired sensitivity and efficiency, crucial for successful implementation in wearable IOP monitoring devices.

The time domain solver in CST is a powerful numerical simulation tool which offers several key advantages; namely a comprehensive dynamic analysis capable of simulating how sensor response to changes in input parameters over time, allowing the sensor's behavior under varying conditions to be documented. Furthermore, the resonance frequency shifts can be investigated in response to alterations in spiral antenna thickness and the number of turns. By comparing simulation results of sensor's with various dimensions, the sensor's design parameters can be fine-tuned. This iterative process ensures the proposed CPS meets desired performance criteria for IOP monitoring applications.

Furthermore, in CST, assigning a waveguide port to an antenna can affect the desired frequency response, several considerations are essential for optimizing the antenna performance and ensuring an efficient frequency response. Firstly, the influence of the waveguide port on the antenna's radiation pattern. The shape and dimensions of the waveguide can impact the antenna's beamwidth, directivity, and gain, all of which affect the frequency response in terms of radiation characteristics. Polarization alignment is also vital in ensuring a uniform frequency response. The waveguide port should be aligned with the desired polarization of the antenna to avoid signal degradation resulting from mismatches in polarization. Waveguide losses can introduce signal attenuation at certain frequencies, influencing the overall frequency response of the antenna system. Lastly, waveguides may exhibit resonant modes at specific frequencies, which can interact with the antenna and impact its frequency response. The waveguide port here is defined in the transverse (z-axis) place to simulate the reader position.

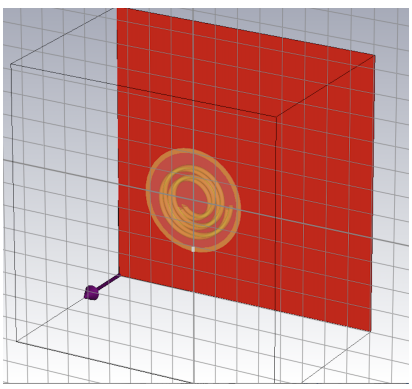

Fig. 6. Wave port guide.

B. Sensor-Antenna under Deformation

An increase in IOP leads to corneal deformation and changes in ocular volume, resulting in deformation of the sensor. This deformation induces a shift in the signal. The objective of this study is to quantify the deformations concerning IOP and investigate the resonance frequency shift that occurs with an increase in IOP. A justification for utilizing spiral sensors is due to the maximum displacement that occurs on the cornea when IOP increases. As seen in Figure 7, the maximum displacement of the eye occurs 2-6mm from the pupil. The maximum displacement shift leads to a more detectable physical change and generates a larger resonance frequency shift, meaning the sensor has improved sensitivity.

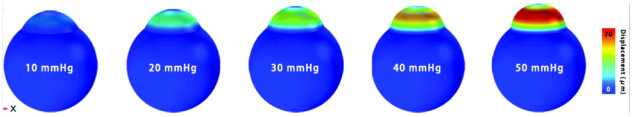

Fig. 7. Displacement in μm of cornea due to IOP increase [29].

C. Simulation set-up

The experimental setup involved adjusting the spiral thickness and turns, resulting in a table with a range of potential designs. A subset of 13 models was randomly selected from this table for simulation using CST. The resonance frequency at both no deflection and induced IOP deflection points was recorded, and the shift in resonance frequency was measured; as well as the Q-factor for each model. Subsequently, four additional runs were randomly generated and selected from the models with the highest resonance frequency shift; these models are labelled as model 10-13 in Table VI. This additional step aimed to identify a model with further improved resonance frequency shift and ultimately determine the design with the largest shift. The randomized selection of runs is listed in Table VI, the full run table can be found in Appendix XIII.

TABLE VI
Randomized selection of runs.

Run	Thickness	Spiral Turns
1	120/500	3
20	310	3
6	120	3
2	100	3
11	200	4
16	300	4
8	120	5
44	500	2.5
27	500	2
51	250	4
52	100	4
53	350	3
54	120	4

IV. Results

A. Pressure Sensor Deflection

The sensitivity of the IOP sensor is directly related to the device displacement and the air gap between the two plates of the capacitor. Therefore, it is necessary to ensure a linear pressure response in the pressure range of 0–60 mmHg so that the resonance frequency shift can be correlated with a specific IOP increase. Figure 18 shows the maximum deflection at the center of the sensor using COMSOL Multiphysics. The deflection is linear in the relevant region of 0-8000 Pa (0-60mmHg).

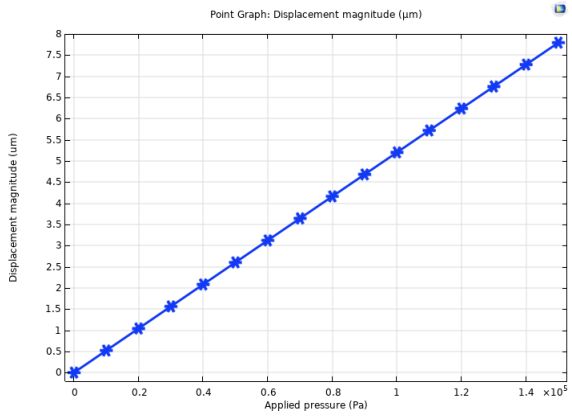

Fig. 8. Deflection of device with induced pressure using COMSOL Multiphysics

The deflection of 3 designs was simulated to ensure linear response in the relevant pressure region; specifically with spiral thickness of 120 μm, 310 μm, and 500 μm. All three models experienced the same values of deflection with respect to the induced IOP. This result allowed the same deflection to be induced in CST Studio Suite. Table VII shows the displacement at no induced pressure and maximum IOP pressure at the center point of maximum deflection. The full data table ranging from 0-8000 Pa for all three designs can be found in appendix VI-B.

TABLE VII
The points of maximum and minimum induced pressure deflection of three designs.

Induced pressure (Pa)	Design 1 displacement (um)	Design 2 displacement (um)	Design 3 displacement (um)
0	1.332e-10	4.189e-9	1.332e-10
8000	4.163	4.592	4.164

B. Resonance Frequency Shift

The model is characterized using S_{11} to analyze the performance of wireless data transfer. The operating frequency from the simulation is approximately 4.1 GHz, while the gain of the sensor-antenna is 3 dB. Figure 9 and 10 display the resonance frequency shift in GHz related to the spiral thickness and number of turns in each model. The model

with maximum resonance frequency shift consists of 3 spiral turns with 350 μm thickness.

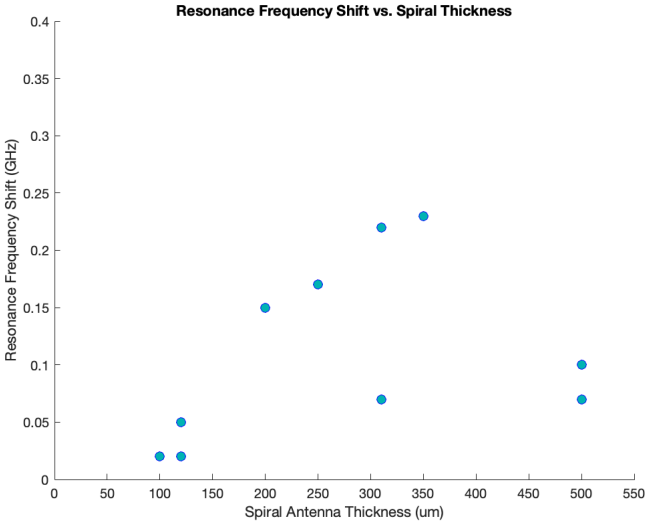

Fig. 9. Resonance frequency shift with respect to the spiral thickness.

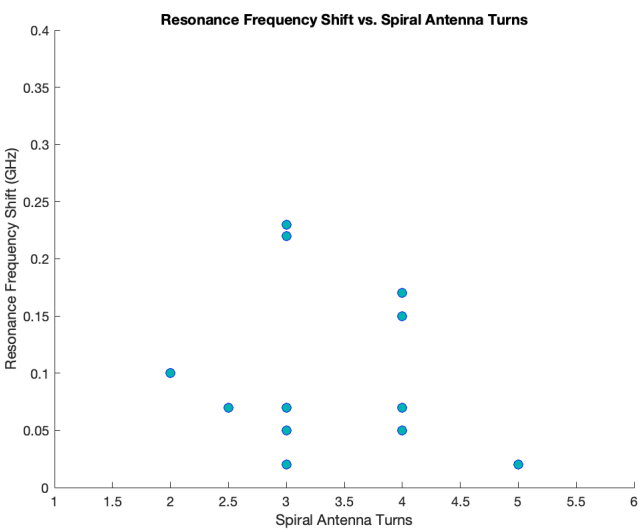

Fig. 10. Resonance frequency shift with respect to the number of spiral turns.

C. Q-Factor results

The Q-factor is calculated with post-processing tools on CST for each design to understand the antenna's efficiency; quantifying the performance of the antenna in terms of resonator bandwidth and energy losses. Figure 11 and 12 display the relating q-factor to each model with varying spiral thickness and turns.

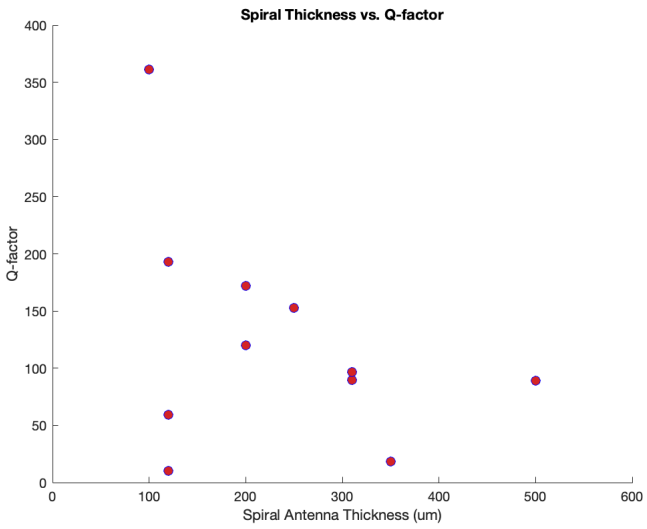

Fig. 11. Q-factor with respect to the spiral thickness.

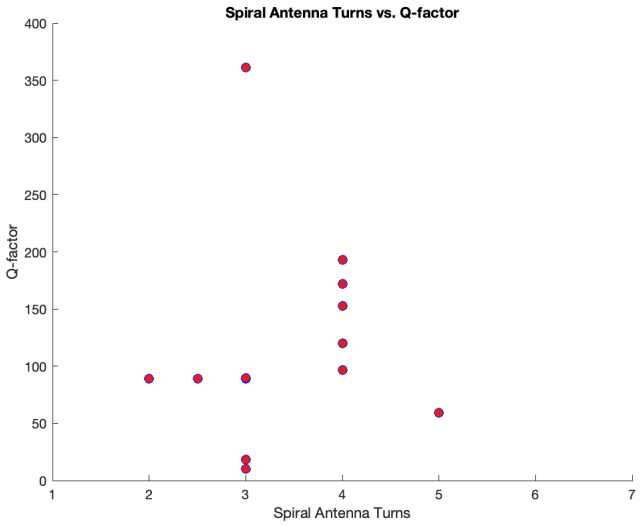

Fig. 12. Q-factor with respect to the number of spiral turns.

D. Highest Sensitivity Design

The 350 μm thickness and three spiral turn design demonstrated the highest sensitivity due to its significant resonance frequency shift which can be seen in Figure 13 and 14.

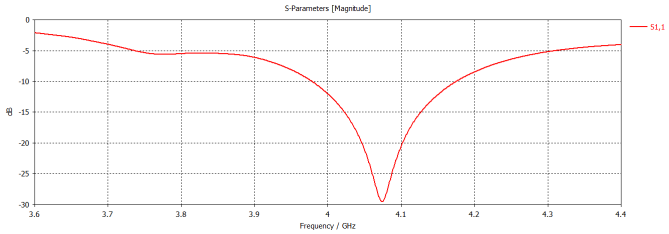

Fig. 13. Reflection coefficient S11 plot of device with highest sensitivity.

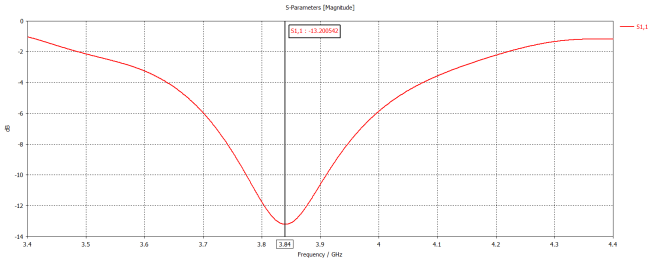

Fig. 14. Reflection coefficient S11 plot of device with highest sensitivity after IOP deflection.

The antenna's measured reflection coefficient (S_{11}) is seen in Figure 13 and 14. A value under -10 dB for S_{11} suggests good operation in the range of interest, 3.9 - 4.1 GHz. The antenna serves as a receiver for wireless power and data transmission, capturing electromagnetic waves emitted from external transmitting terminals, the wireless reader. The reflection coefficient (an S_{11} value of -10 dB or less) corresponds to a higher reflected power ratio. The antenna's bandwidth represents the range over which it efficiently radiates or receives energy, thus when S_{11} $<$ -10 dB it indicates a sharper resonance frequency peak. The model with highest sensitivity is recorded in Table VIII with the original design.

TABLE VIII
Sensitivity of original design and design with largest resonance frequency shift.

Device	**Sensitivity (f_0 shift per mmHg)**	**Q-factor**
Original	2.4 MHz	89.1
Selected Design 53	3.8 MHz	18.4

V. Final Remarks

A. Discussion

The consistent deflection in COMSOL observed across various spiral electrode thicknesses can be attributed to the inherent flexibility and elasticity of the utilized materials, namely Gr-AgNW and Ecoflex. The employment of these flexible and transparent materials distinguishes this device from other ongoing trials involving IOP wearables.

For a wearable lens compared to an implantable lens, the ideal Q-factor range is determined based on specific design requirements and application constraints. As previously mentioned, a lower Q-factor offers better noise immunity and robustness, making the sensor less susceptible to external disturbances. This is advantageous for continuous monitoring and everyday use, minimizing the impact of external factors on the sensor's measurements. In contrast, for an implantable lens, higher Q-factors are generally desired to achieve greater sensitivity and accuracy. Implantable lenses can utilize more complex electronics and external powering, allowing for higher Q-factors without portability or energy consumption concerns. Determining the precise Q-factor requirements involves considering the target pressure range, desired sensitivity, and environmental noise levels.

Q-factor values can fall within a very broad range from 1-1000, or more. A higher Q-factor indicates lower energy losses and increased sensitivity to changes in IOP, enabling more accurate and precise measurements. Table IX compares the device's Q-factor with the highest sensitivity to other wearable IOP sensors, indicating its efficiency. Notably, the proposed design's Q-factor (18.4) aligns with similar sensors in the literature. A Q-factor below 5 is considered low, while above 40 is high; the proposed device fits this desired range. Therefore, the proposed device falls into the desired range.

TABLE IX
Q-factor comparison of the proposed model design with other work.

Device	**Q-factor**
Proposed design	18.4
Original design	89.1
[16]	15
[42]	46.5
[43]	28

The observed improvement in resonance frequency shift in the spiral antenna with 3 turns compared to the original can be attributed to the interplay between the antenna's capacitance and inductance. In CPSs, the resonance frequency is governed by the sensor's capacitance, which is directly related to the area of the spiral antenna. The spiral antenna with 3 turns possesses a smaller area than the one with 5 turns, resulting in reduced capacitance. This lower capacitance contributes to a higher resonance frequency shift during mechanical deformation caused by pressure variations, thereby enhancing sensitivity. Moreover, the number of turns in the spiral antenna influences the sensor's inductance, which, in turn, impacts the Q-factor. A higher number of turns increases inductance, potentially leading to a lower Q-factor for the spiral antenna with 5 turns. Consequently, this may result in a less prominent resonance frequency shift and reduced sensitivity.

The practical application of this device envisions a recommended continuous 24-hour monitoring of IOP at regular intervals over the course of a year. The envisaged

wearable lens-based sensor could be particularly valuable for patients identified as high-risk for glaucoma. These high-risk categories encompass factors such as age, hypertension, sleep apnea, genetic predisposition, and diabetes, among others [44]. The incorporation of such a device could significantly enhance the diagnosis of advanced glaucoma, leading to timely initiation of treatment strategies and consequent reduction in glaucoma-associated blindness.

1) Limitations of Study:

Lack of In-Vitro Testing

In the case of wearable IOP sensors, applanation tonometry is used which infers IOP from the force required to flatten a constant area of the cornea. Therefore, utilizing a wearable lens means a tonometer cannot be used to test the viability of the device. Instead, a pressure sensor must be inserted into the eye, for example TESTO 511; however, this can only be done on animal samples.

Implantation

Owing to the capacitive sensing mechanism of the device, the sensor could be integrated onto a commercial implantable lens. This holds potential benefits for cataract patients undergoing surgery, as the sensor could be directly embedded into the implantable lens, negating the need for a separate procedure. Integrating an IOP sensing device during cataract surgery in senior patients offers a unique opportunity for simultaneous intervention and monitoring. This combined approach minimizes patient discomfort and optimizes postoperative care by addressing both cataracts and elevated IOP in a single procedure. However, limiting the sensor to patients requiring cataract surgery disregards a whole patient category of users who aim to prevent glaucoma and do not require surgery. While minimizing unnecessary surgeries is essential, leveraging the context of cataract surgery in senior patients to accommodate IOP monitoring underscores a pragmatic approach to comprehensive ocular care.

B. Conclusion

The sensor's design incorporates deformable elements, which respond to pressure-induced strain, resulting in changes in the resonant frequency of the sensing LC tank when pressure is applied. analysis of the wireless CPS was designed and presented using CST Studio Suite. The resonance frequency shift at a point of no induced pressure and maximum induced pressure, as well as the Q-factor of various models was simulated. Based on analytical calculations and simulation results, it has been observed that the frequency shift is linked to the alterations of the spiral coil's thickness and number of turns; with the thickness having a larger impact on the resonance frequency shift. However, a precise mathematical equation governing this relationship remains to be fully elucidated. Ongoing research endeavors are focused on investigating alternative designs and their electromagnetic responses to comprehensively understand the fundamental principles behind this relationship and optimize the sensing mechanism. From this study, it can be concluded that utilizing a spiral thickness of 350 μm and 3 spiral turns creates the largest shift of the models designed at 3.8 MHz per mmHg of pressure change, offering an increased shift of IOP detection compared to the original model. The device design also meets the structural criteria required to be fitted onto a wearable commercial lens. However, the fabrication of the design utilizing Gr-AgNW must now be conducted to confirm the realized design. This optimized configuration not only enhances sensitivity but also streamlines the fabrication process by eliminating the need for laborious trial-and-error iterations with different antenna turns and thickness'.

Clinical IOP measurements are prone to errors, including eyelid closure, tear film hypofluorescence, accommodation, eye position and body positioning, leading to inaccuracies. Increasing clinic-based IOP measurements cannot fully address these issues, but continuous ambulatory IOP monitoring shows promise in overcoming these limitations. Initial implementations may target cases with management uncertainties like normal-tension glaucoma, ocular hypertension, and patients with progression despite daytime IOP control. Advanced glaucoma patients at high risk of deterioration could also benefit. Ultimately, 24-hour therapy assessment, as well as improved prevention through early detection, for all glaucoma patients can be achieved through continuous monitoring.

C. Outlook

The multi-disciplinary nature of this project opens portals for various paths to proceed with. The ideal IOP sensing device requires a Gr-AgNW material with optimal transparency and flexibility; an efficient wireless LC-tank circuit; a highly sensitive wearable sensor; and the fabrication of a user-friendly system that integrates all components.

Fabrication

The choice of Silver-Nanowire (AgNW) for the plates is motivated by its flexibility, excellent conductivity, and relatively high transparency, as demonstrated in various pressure sensing devices [45]. Nevertheless, integrating materials like graphene could further enhance optical transmission. For instance, in [46] an IOP sensing device incorporated few-layer graphene sheets, though they encountered a significant initial pressure-induced increase in device resistance. This limitation could be mitigated by increasing the number of graphene layers, albeit at the expense of transparency [46].

The dielectric constant of the Gr-AgNW varies with the amount of graphene incorporated. While higher graphene content enhances the conductivity and increases the dielectric constant, it also comes with elevated costs, making it less suitable for large-scale commercial production. Evaluating the performance of materials with varying graphene content

could allow for improved transparency and decreased cost of production. For example, considering different models to illustrate the trade-offs involved in the optimal sensor design could be conducted prior to fabrication .

A low-graphene model exhibits reduced conductivity and dielectric constant, yielding lower sensitivity. However, it provides cost advantages and relatively high optical transmittance, making it suitable for budget-sensitive applications that prioritize cost over high sensitivity. On the other hand, a high graphene content model features increased conductivity and dielectric constant, ensuring heightened sensitivity for accurate pressure measurements. However, fabrication costs rise significantly, and optical transmittance diminishes. A method to increase transparency could be through novel methods of utilizing single layer graphene which has an optical transmittance of 97% This model suits high-end applications emphasizing sensitivity over cost and optical considerations. While a high graphene device is preferable, the practicality of fabrication and production costs, as well as potential insurance coverage for users, must be assessed for broad accessibility and viability.

Finally, to ensure that the device is not directly exposed to aqueous fluid when used as a lens, it should be encapsulated in Polydimethylsiloxane (PDMS). The sensor should be characterized with and without PDMS encapsulation. Previous studies suggest the offset induced from encapsulation materials to be minimal and can be compensated through calibration before encapsulation; which used a PDMS layer of 4mm [47].

Integration with an Intraocular Lens

Implementation of the CPS on an intraocular lens (IOL) instead of a wearable lens necessitates specific modifications to adapt to the IOL's characteristics. Notably, the size of the IOL varies depending on its placement in the anterior or posterior chamber and is significantly smaller than a commercial wearable lens. Additionally, the CPS design is currently optimized at the point of maximum displacement, as demonstrated in Figure 7, with the spiral antennas positioned at this critical deflection point. However, when integrated into an IOL, the maximum displacement would reduce, resulting in a decreased shift in the spiral antennas and subsequently lower capacitance change, leading to a decrease in the resonance frequency shift. Consequently, adjustments to the sensor's geometry would be imperative to maintain the desired level of sensitivity achieved in this study. Transitioning to an IOL platform could potentially enable the selection of a higher Q-factor, offering enhanced sensor performance, as discussed in the preceding sections.

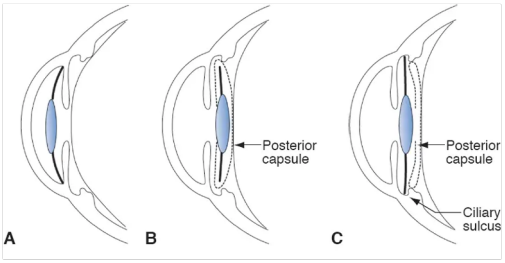

Fig. 15. Image depicting three potential locations for IOLs in the eye a) in the capsular bag in posterior chamber, b) the ciliary sulcus in the anterior chamber [48].

Testing of Fabricated Device

To measure the resonance frequency, the phase dip method can be used. As it would be ideal to have a wireless reader for this sensor at a further distance (fixed on glasses), the phase dip method is suitable to trial this device to achieve a larger telemetry distance. To test the device using the phase dip technique, an external reader antenna should be held coaxial with respect to the spiral sensor, and in proximity of the sensor. Because of inductive coupling between the sensor and readout antenna, a dip of the impedance phase will happen at the sensor's resonance frequency [49]. The maximum possible readout distance between the IOP sensing device and the reader antenna can be determined by increasing the distance of the reader until no dip occurs in the signal. The maximum readout range is directly affected by a low Q-factor of the sensor device. For a better performing wireless link, the sensor coil should have high self inductance, low series resistance, and low parasitic capacitance.

Trialling in Aqueous Humor

The sensor's resonant frequency experiences a decrease when simulated in deionized water due to its high dielectric constant compared to air, which is approximately 80 times greater [50]. Consequently, the device's parasitic capacitance is also influenced by this higher dielectric constant. When the sensor is placed in saline, which is a lossy medium with a complex dielectric constant, the magnitude of the phase dip and the apparent quality factor of the sensor can be assumed to reduce.

REFERENCES

[1] S. Kingman, "Glaucoma is second leading cause of blindness globally," *Bulletin of the World Health Organization*, vol. 82, no. 11, pp. 887–888, 2004.

[2] J. C. DOWNS, M. D. ROBERTS, and C. F. BURGOYNE, "Mechanical environment of the optic nerve head in glaucoma," *Optometry and Vision Science*, vol. 85, no. 6, E425–E435, Jun. 2008. DOI: https://doi.org/10.1097/opx.0b013e31817841cb.

[3] A. Molaei, V. Karamzadeh, S. Safi, H. Esfandiari, J. Dargahi, and M. R. Khosravi, "Upcoming methods and specifications of continuous intraocular pressure monitoring systems for glaucoma," vol. 13, no. 1, pp. 66–66, 2018. DOI: https://doi.org/10.4103/jovr.jovr_208_17.

[4] R. Machiele, M. Motlagh, and B. C. Patel, "Intraocular pressure," 2022. [Online]. Available: https://www-ncbi-nlm-nih-gov.tudelft.idm.oclc.org/books/NBK532237/.

[5] N. Y. Tan, V. Koh, M. J. Girard, and C.-Y. Cheng, "Imaging of the lamina cribrosa and its role in glaucoma: A review," *Clinical & Experimental Ophthalmology*, vol. 46, no. 2, pp. 177–188, 2018.

[6] Y. W. Kim and K. H. Park, "Exogenous influences on intraocular pressure," *The British journal of ophthalmology*, vol. 103, no. 9, pp. 1209–1216, 2019. DOI: 10.1136/bjophthalmol-2018-313381.

[7] R. Buddle, "A day in the life of iop," *Review of Optometry*, vol. 151, no. 12, pp. 26–32, 2014.

[8] N. EHLERS, T. BRAMSEN, and S. SPERLING, "Applanation tonometry and central corneal thickness," *Acta Ophthalmologica*, vol. 53, no. 1, pp. 34–43, May 2009. DOI: https://doi.org/10.1111/j.1755-3768.1975.tb01135.x.

[9] M. M. Whitacre and R. Stein, "Sources of error with use of goldmann-type tonometers," *Survey of Ophthalmology*, vol. 38, no. 1, pp. 1–30, Jul. 1993. DOI: https://doi.org/10.1016/0039-6257(93)90053-a.

[10] J. Liu and C. J. Roberts, "Influence of corneal biomechanical properties on intraocular pressure measurement," *Journal of Cataract and Refractive Surgery*, vol. 31, no. 1, pp. 146–155, Jan. 2005. DOI: https://doi.org/10.1016/j.jcrs.2004.09.031.

[11] S. Srinivasan, N. S. Choudhari, M. Baskaran, R. J. George, B. Shantha, and L. Vijaya, "Diurnal intraocular pressure fluctuation and its risk factors in angle-closure and open-angle glaucoma," *Eye*, vol. 30, no. 3, pp. 362–368, Mar. 2016. DOI: https://doi.org/10.1038/eye.2015.231. [Online]. Available: https://www.ncbi.nlm.nih.gov/pmc/articles/PMC4791692/.

[12] M. S. Dikopf, T. S. Vajaranant, and C. E. Joslin, "Systemic disease and long-term intraocular pressure mean, peak, and variability in nonglaucomatous eyes," vol. 193, pp. 184–196, Sep. 2018.

[13] J. Kim, M. Kim, M.-S. Lee, *et al.*, "Wearable smart sensor systems integrated on soft contact lenses for wireless ocular diagnostics," *Nature Communications*, vol. 8, no. 1, pp. 1–8, 2017. DOI: https://doi.org/10.1038/ncomms14997. [Online]. Available: https://www.nature.com/articles/ncomms14997.

[14] K. Mansouri and T. Shaarawy, "Continuous intraocular pressure monitoring with a wireless ocular telemetry sensor: Initial clinical experience in patients with open angle glaucoma," *British Journal of Ophthalmology*, vol. 95, no. 5, pp. 627–629, Jan. 2011. DOI: https://doi.org/10.1136/bjo.2010.192922.

[15] N. Hernández-Sebastián, D. Díaz-Alonso, F. Renero-Carrillo, N. Villa-Villaseñor, and W. Calleja-Arriaga, "Design and simulation of an integrated wireless capacitive sensors array for measuring ventricular pressure," *Sensors*, vol. 18, no. 9, p. 2781, Aug. 2018. DOI: https://doi.org/10.3390/s18092781.

[16] G.-Z. Chen, I.-S. Chan, L. K. Leung, and D. C. Lam, "Soft wearable contact lens sensor for continuous intraocular pressure monitoring," *Medical Engineering Physics*, vol. 36, no. 9, pp. 1134–1139, Sep. 2014. DOI: https://doi.org/10.1016/j.medengphy.2014.06.005.

[17] G.-Z. Chen, I.-S. Chan, and D. C. Lam, "Capacitive contact lens sensor for continuous non-invasive intraocular pressure monitoring," *Sensors and Actuators A: Physical*, vol. 203, pp. 112–118, 2013.

[18] M. H. M. Kouhani, J. Wu, A. Tavakoli, A. J. Weber, and W. Li, "Wireless, passive strain sensor in a doughnut-shaped contact lens for continuous non-invasive self-monitoring of intraocular pressure," *Lab on a Chip*, vol. 20, no. 2, pp. 332–342, 2020. DOI: https://doi.org/10.1039/c9lc00735k.

[19] M. Hossein, A. J. Weber, and W. Li, "Wireless intraocular pressure sensor using stretchable variable inductor," Jan. 2017. DOI: https://doi.org/10.1109/memsys.2017.7863467.

[20] S. Kwon, S. H. Kim, D. Khang, and J. Y. Lee, "Device profile of the eyemate-io™ system for intraocular pressure monitoring: Overview of its safety and efficacy," *International Journal of Nanomedicine*, vol. 130, no. 15, pp. 5745–5765, 2020. DOI: https://doi.org/10.1001/archophthalmol.2012.2280.

[21] P. Vitish-Sharma, A. G. Acheson, R. Stead, *et al.*, "Can the sensimed triggerfish® lens data be used as an accurate measure of intraocular pressure?" *Acta Ophthalmologica*, vol. 96, no. 2, e242–e246, 2017. DOI: https://doi.org/10.1111/aos.13456.

[22] A. Agarwal, A. Shapero, D. Rodger, M. S. Humayun, Y. Tai, and A. Emami, "A wireless, low-drift, implantable intraocular pressure sensor with parylene-on-oil encapsulation," *California Institute of Technology*, 2018. DOI: https://doi.org/10.1109/cicc.2018.8357049.

[23] I. Clausen and T. Glott, "Development of clinically relevant implantable pressure sensors: Perspectives and challenges," *Sensors*, vol. 14, no. 9, pp. 17 686–17 702, Sep. 2014.

[24] J. O. Lee, H. Park, J. Du, *et al.*, "A microscale optical implant for continuous in vivo monitoring of intraocular pressure," *Microsystems Nanoengineering*, vol. 3, no. 1, pp. 1–9, Dec. 2017. DOI: https://doi.org/10.1038/micronano.2017.57. [Online]. Available: https://www.nature.com/articles/micronano201757.

[25] K. C. Katuri, M. K. Ramasubramanian, and S. Asrani, "A surface micromachined capacitive pressure sensor for intraocular pressure measurement," Jul. 2010. DOI: https://doi.org/10.1109/mesa.2010.5552077.

[26] M. Leonardi, E. M. Pitchon, A. Bertsch, P. Renaud, and A. Mermoud, "Wireless contact lens sensor for

intraocular pressure monitoring: Assessment on enucleated pig eyes," *Acta Ophthalmologica*, vol. 87, no. 4, pp. 433–437, Jun. 2009. DOI: https://doi.org/10.1111/j.1755-3768.2008.01404.x.

[27] Z. Ma, Y. Zhang, K. Zhang, H. Deng, and Q. Fu, "Recent progress in flexible capacitive sensors: Structures and properties," *Nano Materials Science*, 2022.

[28] H. An, L. Chen, X. Liu, B. Zhao, H. Zhang, and Z. Wu, "Microfluidic contact lenses for unpowered, continuous and non-invasive intraocular pressure monitoring," *Sensors and Actuators A: Physical*, vol. 295, pp. 177–187, 2019. DOI: 10.1016/j.sna.2019.04.050.

[29] Z. Dou, J. Tang, Z. Liu, *et al.*, "Wearable contact lens sensor for non-invasive continuous monitoring of intraocular pressure," *Micromachines*, vol. 12, no. 2, 2021.

[30] J. T. Wilensky, "Diurnal variations in intraocular pressure.," *Transactions of the American Ophthalmological Society*, vol. 89, pp. 757–790, 1991. [Online]. Available: https://www.ncbi.nlm.nih.gov/pmc/articles/PMC1298639/.

[31] E. Chihara, "Assessment of true intraocular pressure: The gap between theory and practical data," *Survey of Ophthalmology*, vol. 53, no. 3, pp. 203–218, 2008. DOI: https://doi.org/10.1016/j.survophthal.2008.02.005.

[32] B. K. Pierscionek, M. Asejczyk-Widlicka, and R. A. Schachar, "The effect of changing intraocular pressure on the corneal and scleral curvatures in the fresh porcine eye," *The British Journal of Ophthalmology*, vol. 91, no. 6, pp. 801–803, Jun. 2007. DOI: https://doi.org/10.1136/bjo.2006.110221. [Online]. Available: https://www.ncbi.nlm.nih.gov/pmc/articles/PMC1955613/.

[33] "Diabetic retinopathy," *National Institute of Health*, 2022. [Online]. Available: https://www.nei.nih.gov/.

[34] *AVNET*, [Online]. Available: https://www.avnet.com/.

[35] A. M. Niknejad, *Electromagnetics for High-Speed Analog and Digital Communication Circuits*. Cambridge University Press, Feb. 2007, ISBN: 9781139462242.

[36] D. Kajfez, "Q factor measurements , analog and digital," 1999. [Online]. Available: https://api.semanticscholar.org/CorpusID:1929698.

[37] K. Cao, H. Yang, L. Gao, *et al.*, "In situ mechanical characterization of silver nanowire/graphene hybrids films for flexible electronics," *International Journal of Smart and Nano Materials*, vol. 11, no. 3, pp. 265–276, 2020.

[38] J. Shintake, H. Sonar, E. Piskarev, J. Paik, and D. Floreano, "Soft pneumatic gelatin actuator for edible robotics," pp. 6221–6226, 2017. DOI: 10.1109/IROS.2017.8206525.

[39] M. Sang, J. Shin, K. Kim, and K. Yu, "Electronic and thermal properties of graphene and recent advances in graphene based electronics applications," *Nanomaterials*, vol. 9, no. 3, p. 374, Mar. 2019. DOI: https://doi.org/10.3390/nano9030374.

[40] A. Elements, "Silver nanowires," *American Elements*, [Online]. Available: https://www.americanelements.com/silver-nanowires-7440-22-4.

[41] G. Jing, H. Duan, X. Sun, *et al.*, "Surface effects on elastic properties of silver nanowires: Contact atomic-force microscopy," *Physical Review B*, vol. 73, no. 23, Jun. 2006. DOI: https://doi.org/10.1103/physrevb.73.235409.

[42] H. Zhu, H. Yang, L. Zhan, Y. Chen, J. Wang, and F. Xu, "Hydrogel-based smart contact lens for highly sensitive wireless intraocular pressure monitoring," *ACS Sensors*, vol. 7, no. 10, pp. 3014–3022, Oct. 2022. DOI: https://doi.org/10.1021/acssensors.2c01299.

[43] J.-W. Lin, Y. Zhao, P.-J. Chen, and Y.-C. Tai, "High quality factor parylene-based intraocular pressure sensor," *Nano/Micro Eng. Mol. Syst.*, Mar. 2012. DOI: https://doi.org/10.1109/nems.2012.6196741.

[44] C. W. McMonnies, "Glaucoma history and risk factors," *Journal of Optometry*, vol. 10, no. 2, pp. 71–78, 2017.

[45] F. Basarir, Z. Madani, and J. Vapaavuori, "Recent advances in silver nanowire based flexible capacitive pressure sensors: From structure, fabrication to emerging applications," *Advanced Materials Interfaces*, vol. 9, no. 31, p. 2 200 866, 2022.

[46] J. Xu, T. Cui, T. Hirtz, *et al.*, "Highly transparent and sensitive graphene sensors for continuous and non-invasive intraocular pressure monitoring," *ACS Applied Materials & Interfaces*, vol. 12, no. 16, pp. 18 375–18 384, 2020.

[47] T. Kakaday, M. Plunkett, Steven, J. S. Jimmy, N. H. Voelcker, and J. E. Craig, "Development of a wireless intra-ocular pressure monitoring system for incorporation into a therapeutic glaucoma drainage implant," *Biomedical Applications of Micro- and Nanoengineering IV and Complex Systems*, Dec. 2008. DOI: https://doi.org/10.1117/12.810647.

[48] *www.aao.org*, [Online]. Available: https://www.aao.org/education/bcscsnippetdetail.aspx?id=c34bb31f-3f12-48fc-b90b-0f0a3d9d37b1.

[49] B. Crum and W. Li, "Parylene-based fold-and-bond wireless pressure sensor," pp. 1155–1158, 2013. DOI: 10.1109/NEMS.2013.6559926.

[50] *www.chemeurope.com*, [Online]. Available: https://www.chemeurope.com/en/encyclopedia/Deionized_water.html.

[51] *rvaf.com*, [Online]. Available: https://rvaf.com/treatments/dislocated_iol.php.

[52] S. Stevens, C. Gilbert, and N. Astbury, "How to measure intraocular pressure: Applanation tonometry," *Community Eye Health*, vol. 21, no. 66, pp. 74–75, 2008.

[53] A. M. Bhorade, M. O. Gordon, B. Wilson, R. N. Weinrab, and M. A. Kass, "Variability of intraocular pressure measurements in observation participants in

the ocular hypertension treatment study," *Ophthalmology*, vol. 116, no. 4, pp. 717–724, Apr. 2009. DOI: https://doi.org/10.1016/j.ophtha.2008.12.036.

VI. Appendix

A. Device Comparison

Device	Sensitivity	Thickness	Diameter (mm)	Detectable pressure range (mmHg)	Resonance frequency	Drawbacks	Source
Sensing channel connected to liquid and air reservoir. Increase in IOP causes increases microfluid reservoir volume, vacuum created and sucks interface to liquid chamber.	106 µm/mmHg	150 um	15.5	10-40	n/a	Relatively stiff, but stability decreases with increasing flexibility of materials.	10.1039/c8lc00758f
Ring-shaped with two parts: MEMS ASIC chip and a microcoil antenna. IOP recording = array of capacitive pressure sensors. 2 parallel plates with thin flexible membrane indented by IOP and thick rigid base. Analog signal produced as capacitance changes across sensors.	7000 ppm/mmHg	0.9 mm	11.3	0-45	13.56 MHz	Risk of anterior iris displacement, pigmentary glaucoma, IO fibrosis	10.1167/ iovs.11-7878 10.1001/jamaophthalmol.2014.1739 10.1080/17434440.2020.1761788
An LC-resonator strain sensor placed in a wearable lens, made of stretchable inductance coil using a liquid-metal and chip capacitor. Stretchable inductor coil made chip capacitor. Increase in IOP stretches inductance coils, decreasing resonant frequency.	78.9-86.7 KHz/mmHg	n/a	14	0-36 mmHg	190 MHz	Q-coefficient decreases by 18% due to resistance increase of the liquid metal due to oxidation	10.1088/1361-6439/abd8e0
Graphene Wheatstone bridge with 2 strain gauges and 2 resistors made on a wearable lens.	150 uV/mmHg	n/a	13.5	0-55	n/a	Initial graphene-Wheatstone resistance. Thick, cause discomfort.	10.1021/acsami.0c02991
Wireless, flexible passive IOP sensor which uses a planar stretchable variable inductor to record strain on the sclera. Uses inductive coupling to external coil.	57 kHz/mmHg	10um (no encapsulation)	14	0-70	551 MHz	No sealed chamber used, removes inaccuracy overtime due to baseline drift. Not-transparent, zig-zag visible sensory coil sits on eye	10.1016/j.medengphy.2014.06.00
Ultra low power wireless IOP sensor that uses a relaxation oscillator to convert capacitance to frequency. RF backscatter is used for measured sample computing. Device includes an antenna, pressure sensor and IC. For IOP sensing a capacitive MEMS sensor is used. The oscillator-based convertor modulates backscatter to the reader. Chip implant.	f 1.6 fF/mmHg	n/a	1x0.7mm2	0-67 mmHg	2.4 GHz	6.7 mmHg readout error if not calibrated	10.1109/JSSC.2011.2164134
Transparent Gr-AgNW capacitive pressure sensor passivated with parylene. 2 Gr-Ag-Nanowires used as sensor electrode plates and antennas for wireless read-out.	2.2 MHz/mmHg	0.756 um	11mm	5-50 mmHg	4.1 GHz	Limited simulation and testing discussed, IOP and glucose recording done in parallel	10.1038/ncomms14997
Wireless, flexible, passive pressure sensor made of an integrated MEMS coil and variable capacitor. Device operates as resonant LC circuit using 3-turn inductor, the end are compacted into a parallel plate capacitor. Then sealed, so a chamber is created and its volume depends on component rigidity and IOP. When capacitor plates move in response to IOP, capacitance changes, shifting the resonance frequency.	0.156 MHz/mmHg	n/a	15	1-100 mmHg	200 MHz	Not transparent, large. Requires surgery	10.1109/NEMS.2013.6559926

Fig. 16. Comparison of IOP sensing devices

Device	Sensitivity	Thickness	Diameter (mm)	Detectable pressure range (mmHg)	Resonance frequency	Drawbacks	Source
Soft contact lens with strain gauge sensor and an embedded telemetry chip. Measures changes around corneoscleral junction of the eye and transmits them through an antenna. Strain gauge detects ocular volume changes where 1 mmHg change leads to 3um corneal curvature change. Device simulated by 11uA current, gives output voltage that is proportional to strain in strain gauges, and the IOP fluctuations.	Not published	0.6 mm	14.4	5-30	Not published	weak correlation of the Triggerfish lens. Device assumes IOP changes lead to proportional ocular volume and dimension changes.	10.1097/IJG.0b013e318241b874 10.2147/OPTH.S109708
Platinum strain gauge sensor on a wearable lens. Utilizes a wheatstone bridge (2 strain and 2 reference resistances). Pt strain gauge coated in insulating layer and then encapsulated in PDMS. The strain resistances are placed in a circular coil shape and the reference resistance are placed radially, minimal change with IOP increase. So, output voltage is related linearly to IOP fluctuations.	289.5 uV/mmHg	n/a	14	16.5-35	n/a	Visible on eye, potential optical hindrance for patients	10.3390/mi12020108
Thin, stretchable wearable lens has an embedded ocular tonometer which is stretched radially and compressed axially. Sensing component bonded to commercial lens with PDA in-situ polymerization. Sensor is a serpentine ring shape on the periphery of the lens. Inductance and capacitance increase in RLC resonant circuit with IOP increase, leads to decrease in resonance frequency.	0.27 MHz/mmHg	1.004 mm	13	0-40	239 MHz	Visible on eye, potential optical hindrance for patients	10.1038/s41467-022-33254-4
Photonic-crystal based membrane where the lattice distance varies according to morphology changes induced by IOP. Sensor made of opal nanostructure embedded in PDMS. A microhydraulic amplification system is used to increase device sensitivity by increasing the color change range. The system contains silicone oil which is sealed with a PC and parylene membrane. IOP causes deflection due to the fluid pressure. Reflected wavelength shifts wrt. IOP. Deflection amplified by Pascals principle. Membrane color change recorded using a smartphone and quantified. Colors of sensing material assigned RGB value, so each color refers to specific IOP.	Wavelength shift from 596-573 nm. Sensitivity of 0.4 nm/mmHg.	0.3 mm	20	0-80	n/a	Demand for device limited, could be used as a warning when IOP too high; expensive, implementation plan difficult.	10.1039/c9lc01268k
A theranostic wireless lens with a sensitive gold hollow nanowire based IOP sensor. Also incorporates a flexible DDS to treat glaucoma. Circular sensor design which detects resistance change of material when IOP causes radial deformation.	3 mmHg resolution, sensitivity not published	0.65 mm	7.5	0-35	n/a	Produced for rabbit eye, using rabbit anatomical dimensions only. Visible gold components, unaesthetic.	10.1038/s41467-022-34597-8
Wireless absolute capacitive pressure sensor made of a 24-turn gold electroplated coil and capacitive sensor. A thin silicon diaphragm on the metal electrode has a changing capacitance when IOP increases. Not specified for IOP, could be used on IOL.	120 kHz/mmHg	0.006 mm	2.6x1.6mm	0-50	100 MHz	Low operational distance and low q-factor coils.	10.1016/S0924-4247(01)00753-1

Fig. 17. Comparison of IOP sensing devices continued

B. COMSOL Multiphysics Simulations

The model deflection simulated in COMSOL Multiphysics can be seen in Figures 18, 19 and 20, and the data of deflection values can be seen below each plot. COMSOL version 6.1 and CST Studio Suite 2022 were used, under the TU Delft License.

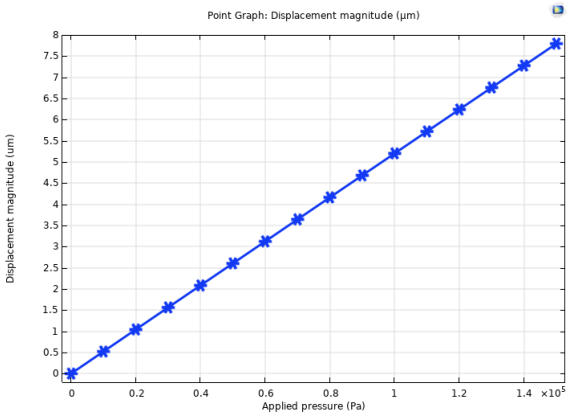

Fig. 18. Displacement 120um thickness.

TABLE X
Displacement data of 120um thick spiral from COMSOL Multiphysics.

Model:	design 1 120umx120um
Version:	COMSOL 6.1.0.357
Date:	Jul 24 2023, 12:20
Dimension:	1
Nodes:	16
Expressions:	1
Description:	Point graph
p0 (Pa)	Displacement magnitude
0	1.3320775036644632E-10
10000	0.5212116802206045
20000	1.0420835350474962
30000	1.5629504088331336
40000	2.0834610593196627
50000	2.603966749554335
60000	3.124099959312323
70000	3.644228231267868
80000	4.163967917023364
90000	4.683702687803716
100000	5.203032923386593
110000	5.7223582679178415
120000	6.241263291058031
130000	6.760163449187487
140000	7.278627666780876
150000	7.797087045863268

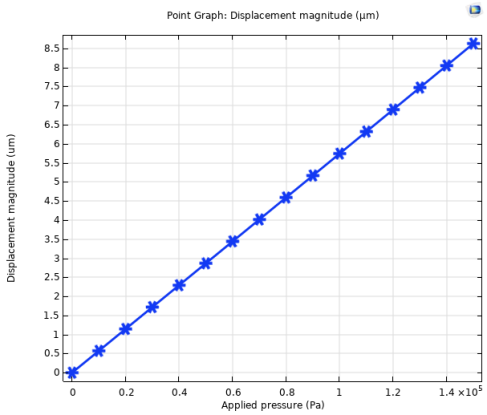

Fig. 19. Displacement 310um thickness.

TABLE XI
Displacement data of 310um thick spiral from COMSOL Multiphysics.

Model:	design 2 310um_pressure sensor
Version:	COMSOL 6.1.0.357
Date:	Jul 24 2023, 12:14
Dimension:	1
Nodes:	16
Expressions:	1
Description:	Point graph
p0 (Pa)	Displacement magnitude
0	4.188582815342255E-9
10000	0.5724376054982344
20000	1.1457276734365214
30000	1.7190108883533046
40000	2.29310092479427
50000	2.8671839812520807
60000	3.4420275028721963
70000	4.016863925147706
80000	4.592413780122135
90000	5.167956423579918
100000	5.744164837151214
110000	6.320365935383916
120000	6.897184557823539
130000	7.4739957695075425
140000	8.051375727883809
150000	8.628748188150722

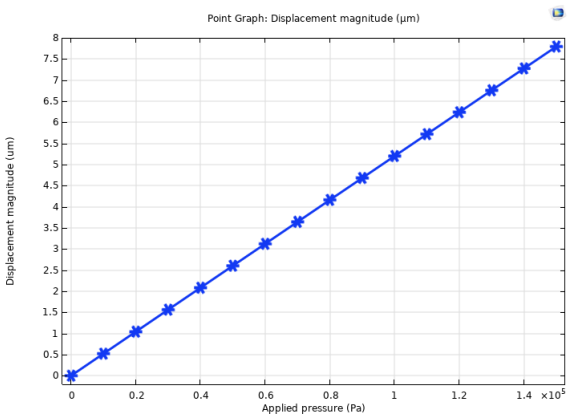

Fig. 20. Displacement data of 500 thick spiral from COMSOL Multiphysics.

TABLE XII

Model:	design 3 500umx500um
Version:	COMSOL 6.1.0.357
Date:	Jul 24 2023, 12:28
Dimension:	1
Nodes:	16
Expressions:	1
Description:	Point graph
p0 (Pa)	Displacement magnitude
0	1.3320775036644632E-10
10000	0.5212116802206045
20000	1.0420835350474962
30000	1.5629504088331336
40000	2.0834610593196627
50000	2.603966749554335
60000	3.124099959312323
70000	3.644228231267868
80000	4.163967917023364
90000	4.683702687803716
100000	5.203032923386593
110000	5.7223582679178415
120000	6.241263291058031
130000	6.760163449187487
140000	7.278627666780876
150000	7.797087045863268

C. Methodology

The experimental design follows Box and Wilson's response surface methodology (RSM) to determine optimal parameters using statistical methods. RSM helps avoid time-consuming trial-and-error attempts. This study utilizes RSM to find the ideal response (maximum Q factor and sensitivity at two distances) for the proposed capacitive pressure sensor by altering its dimensions and spiral revolutions.

To optimally design the experiment, the number of sensor models to be included depends on the parameters considered. A preliminary study defines these parameters and their ranges.

TABLE XIII: Full run table.

Run	**Thickness**	**Spiral Turns**	**Factorial/Axial point**
1	100	2	Factorial Point
2	100	3	Factorial Point
3	100	4	Factorial Point
4	100	5	Factorial Point
5	100	6	Factorial Point
6	120	3	Factorial Point
7	120	4	Factorial Point
8	120	5	Factorial Point
9	200	2	Factorial Point
10	200	3	Factorial Point
11	200	4	Factorial Point
12	200	5	Factorial Point
13	200	6	Factorial Point
14	300	2	Factorial Point
15	300	3	Factorial Point
16	300	4	Factorial Point
17	300	5	Factorial Point
18	300	6	Factorial Point
19	310	2	Factorial Point
20	310	3	Factorial Point
21	310	4	Factorial Point
22	400	2	Factorial Point
23	400	3	Factorial Point

24	400	4	Factorial Point
25	400	5	Factorial Point
26	400	6	Factorial Point
27	500	2	Factorial Point
28	500	3	Factorial Point
29	500	4	Factorial Point
30	500	5	Factorial Point
31	500	6	Factorial Point
32	250	3	Factorial Point
33	250	4	Factorial Point
34	250	5	Factorial Point
35	200	2.5	Factorial Point
36	200	3.5	Factorial Point
37	200	4.5	Factorial Point
38	300	2.5	Factorial Point
39	300	3.5	Factorial Point
40	300	4.5	Factorial Point
41	400	2.5	Factorial Point
42	400	3.5	Factorial Point
43	400	4.5	Factorial Point
44	500	2.5	Factorial Point
45	500	3.5	Factorial Point
46	400	4.5	Factorial Point
47	200	4	Axial Point (ta)
48	400	4	Axial Point (+a)
49	300	2	Axial Point (+a)
50	300	6	Axial Point (+a)
51	250	4	Extra
52	100	4	Extra
53	350	3	Extra
54	120	4	Extra

D. CST Studio Suite

1) Sensor design and model: The sensor was designed in CST following the steps below, detailing the method used for all models, the only variables changed were the spiral thickness and number of turns.

- Geometry creation of the silicone dielectric layer by using a cylinder set to a thickness of 50um.
- Spiral circular coil selected from pre-defined macros, wire radius, inner spiral radius, number of turns are defined here.
- Material assignment form library component, Gr-AgNw and Ecoflex were selected by altering the pre-defined silicon and silver to match the criteria defined in Table IV.
- Define the waveguide port for the device on the outer coil, Macro, solver, calculate port extension coefficient. Define the width of field line, height of substrate and epsilon. Accuracy defined at -30 dB.
- Time-domain solver ran at -30dB accuracy to simulate the sensor's dynamic behavior. This solver allows for transient analysis and records the resonant frequency and q-factor of the device.
- Post-processing: Resonance frequency of the device can be viewed in 1D results, and the q-factor is calculated. The q-factor calculation analyzes the resonance characteristics of the sensor's LC circuit. It quantifies the sharpness of the resonance peak in the frequency response of the sensor and is an indication of how efficiently the sensor is able to store and release energy during resonance. The time-domain solver calculates the transient response of the LC circuit and considers interactions between the spiral antennas and the dielectric silicone layer, as well as the surrounding environment.

2) Simulation Full Results Table:

Table XIV below includes the design parameters for all individual models, as well as the outcome of the resonance frequency recordings and q-factor values.

TABLE XIV: Full results table.

	Deflection	**Spiral thicknes top (um)**	**Spiral thickness bottom (um)**	**Number of turns**	**Q-factor**	**Resonance frequency (GHz)**	**F0 (GHz)**
Design 1 (original)	No induced IOP	120	500	3	89.1	4.11	0.07
	Induced maximum deflection	120	500	3		4.04	
Design 2	No induced IOP	310	310	3	89.83	4.10	0.22
	Induced maximum deflection	310	310	3		3.88	
Design 3	No induced IOP	120	120	3	10.26	4.03	0.05
	Induced maximum deflection	120	120	3		3.98	
Design 4	No induced IOP	100	100	3	361.00	4.23	0,02
	Induced maximum deflection	100	100	3		4.21	
Design 5	No induced IOP	200	200	4	120.00	3.99	0.15
	Induced maximum deflection	200	200	4		3.84	
Design 6	No induced IOP	300	300	4	96.75	4.11	0.07
	Induced maximum deflection	300	300	4		4.04	
Design 7	No induced IOP	120	120	5	59.10	4.11	0.02
	Induced maximum deflection	120	120	5		4.09	
Design 8	No induced IOP	500	500	2.5	89.10	4.11	0.07
	Induced maximum deflection	500	500	2.5		4.04	
Design 9	No induced IOP	500	500	2	89.10	4.04	0.1
	Induced maximum deflection	500	500	2		3.94	
Design 10 - 51	No induced IOP	250	250	4	152.70	4.18	0.17
	Induced maximum deflection	250	250	4		4.01	

Table XIV continued from previous page

Design 11 - 52	No induced IOP	100	100	4	172.00	3.99	0.15
	Induced maximum deflection	100	100	4		3.84	
Design 12 - 53	No induced IOP	350	350	3	18.40	4.07	0.23
	Induced maximum deflection	350	350	3		3.84	
Design 13 - 54	No induced IOP	120	120	4	193.10	3.81	0.05
	Induced maximum deflection	120	120	4		3.56	

E. IOL Types

There is a wide variety of IOLs depending on the need for them being used. The existing IOLs are: toric IOLs, aspheric IOLs, Accommodating IOLs (aIOLs), monofocal IOLs and multifocal IOLs. All of these lenses are treatment options for cataract surgery which involves removing the eye's natural lens are replacing it with one of the IOL options. The natural lens can become damaged overtime and therefore hinder vision in aging patient. Each of these IOLs offers differing benefits such as treatment for far- vs. near-sighted patients, astigmatism, etc.

IOLs can also be either iris-fixated (average diameter of 8.5mm) or placed in the capsular bag. An iris-fixated lens, as described, involves suturing the lens to the iris itself; they can be positioned anterior or posterior to the iris. Figure 21 shows the capsular bag anatomy. Whilst iris-fixation appears a viable option, it is not favored by surgeons due to the lack of suturing being presently conducted in the medical field [5], as well as the difficulty to remove in the future which can be necessary due to the increased risk of dislocation with this type of procedure. For this reason, the IOLs considered are those implanted in the capsular bag, which typically are 8-9mm with haptics for stabilizations.

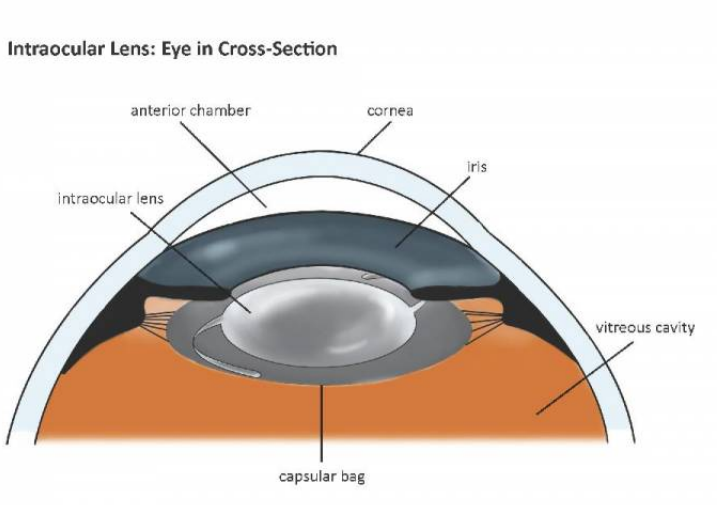

Fig. 21. Schematic displaying an IOL placement in a capsular bag [51].

F. Addressing Common Questions

Slippage of the Lens on Eye Surface

Despite the potential impact of interface slippage between the contact lens and the eye's surface, the frequency responses to intraocular pressure changes remained consistent in initial studies conducted by Kim et al. Notably, the device demonstrated robust performance even when it slipped to different locations on the eyeball. This can be attributed to the presence

[5]this insight was kindly provided by an ophthalmologist from Erasmus MC; details available upon request

of a protective layer, effectively preventing direct contact between the active components of the device and the eyeball. The study validates the consistent frequency responses even in the presence of slippage, underscoring the significance of the protective layer in ensuring stable and accurate pressure readings. Thus, based on the consistent frequency responses observed despite slippage, it can be assumed that the presented CPS, with its utilization of the same materials and minor dimensional changes, would justifiably experience comparable and reliable readings in terms of resonance frequency shift during practical usage.

Intraocular Pressure in Left vs. Right Eye

GAT is used for both the left and right eye, where an ophthalmologist manually places a tonometer on the patient's eye, reading a dial, and records the measurements for each eye [52]. However, this approach is time-consuming for medical staff and only provides insights into a fraction of IOP fluctuations throughout the day. In line with GAT's bilateral assessment, the proposed CPS is envisioned to be placed in both eyes to monitor IOP variations. Despite extensive studies on IOP fluctuations, the underlying causes and mechanisms remain not fully elucidated. An investigation illustrates the variability of IOP recordings between the left and right eyes in patients. This variability cannot be solely attributed to actual IOP increases, tonometer calibration differences, or systemic changes [53]. By employing the CPS in both eyes, it is expected to capture a more comprehensive and continuous profile of IOP changes, providing valuable data to further explore and understand the dynamic nature of IOP fluctuations.

G. Model Overview

Attached on following page.

Model 1: Original

Thickness top spiral: 500um

Thickness bottom spiral: 120um

Spiral turns: 3

Bottom-view	Cross-section
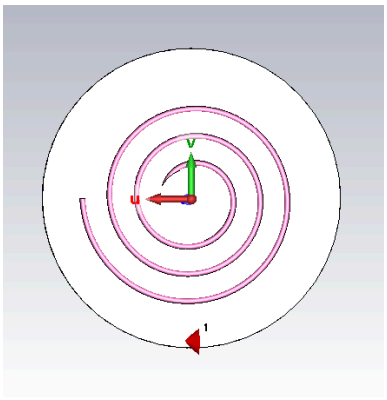	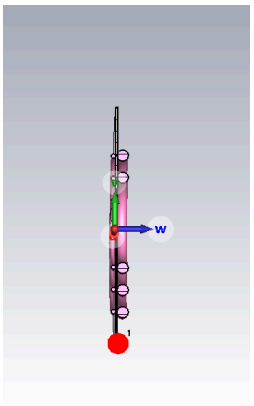

Resonance frequency at 0 IOP: (bandwidth = 170MHz)

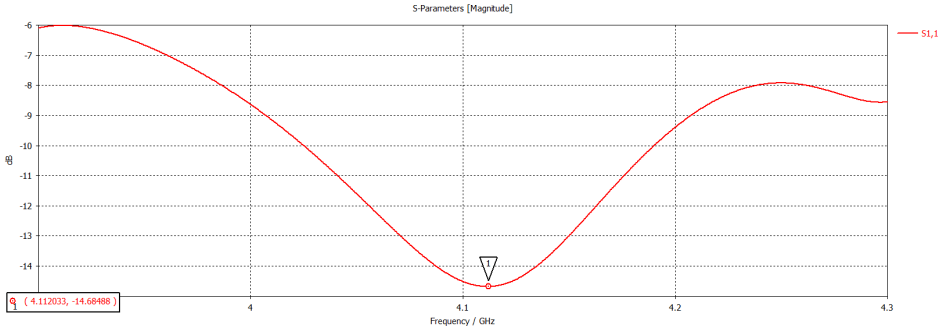

Resonance frequency at maximum IOP:

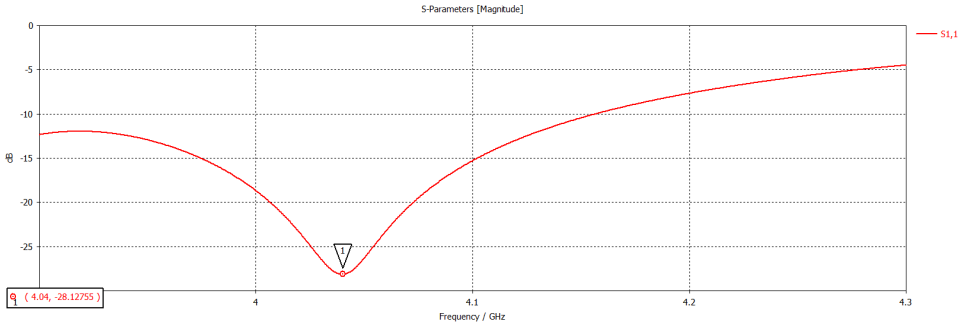

Model 2:

Top-view	Cross-section
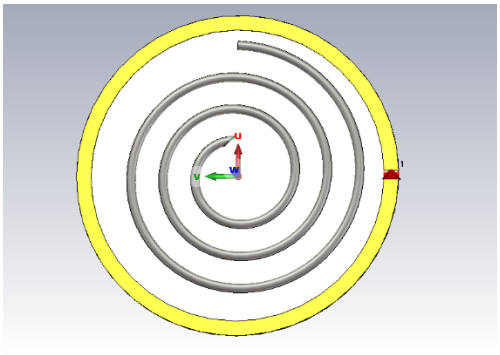	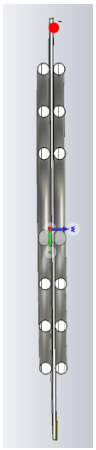

Resonance frequency:

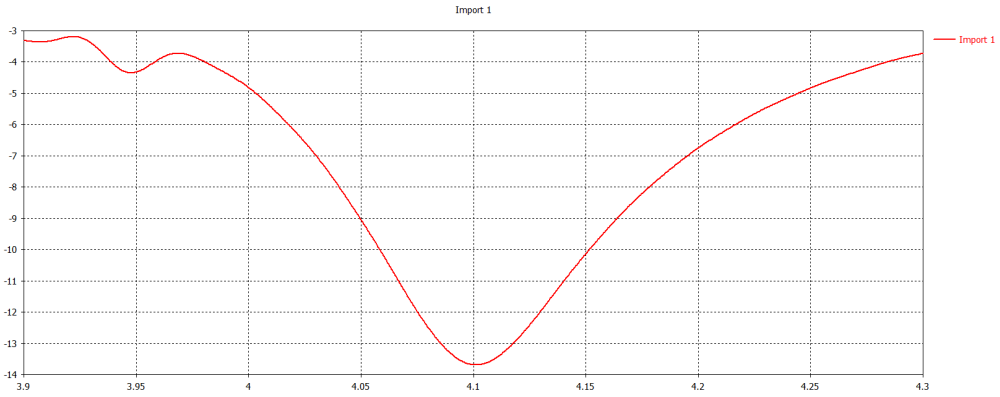

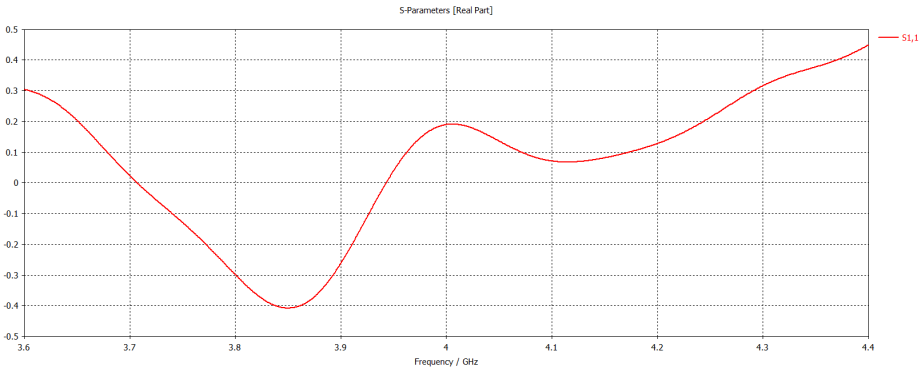

Model 3:

Top-view	Cross-section
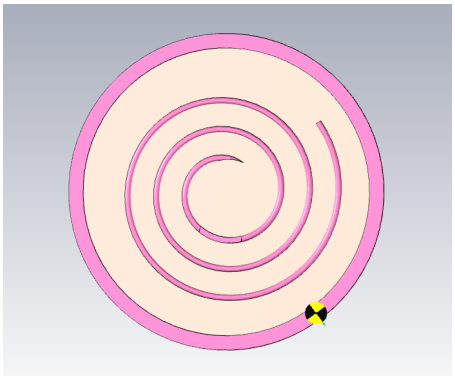	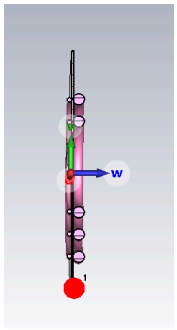

Resonance frequency: (Bandwidth = 210 MHz)

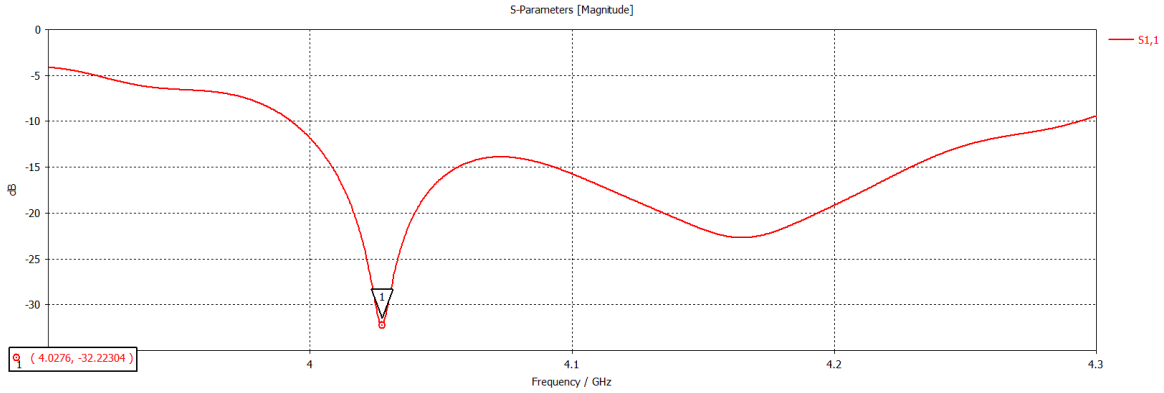

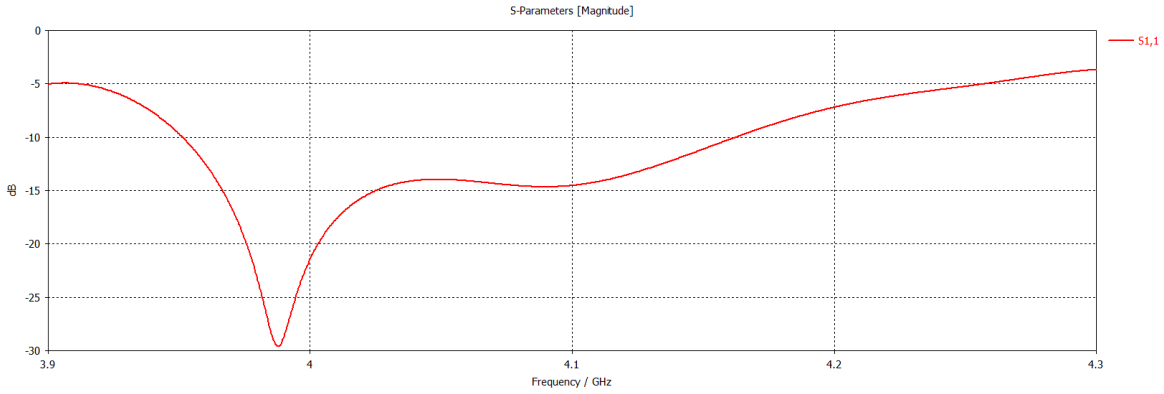

Model 4:

Top-view	Cross-section
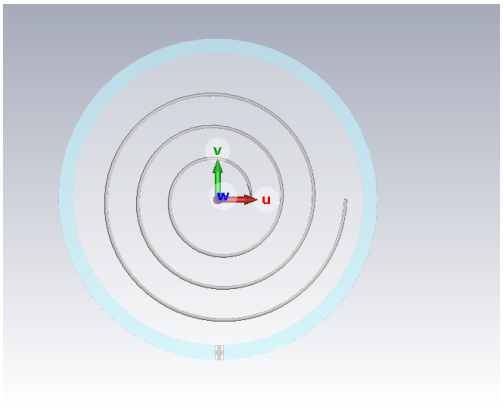	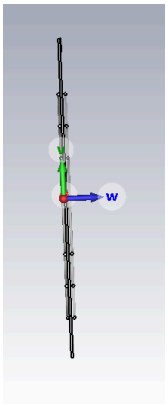

Resonance frequency:

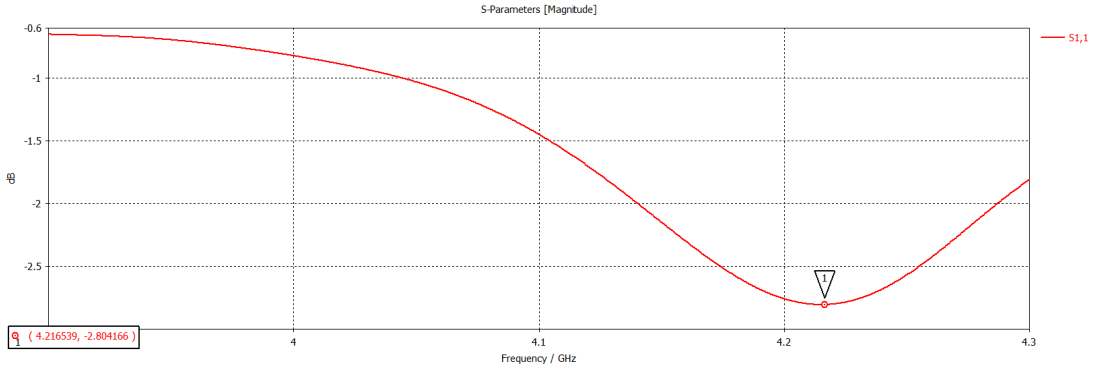

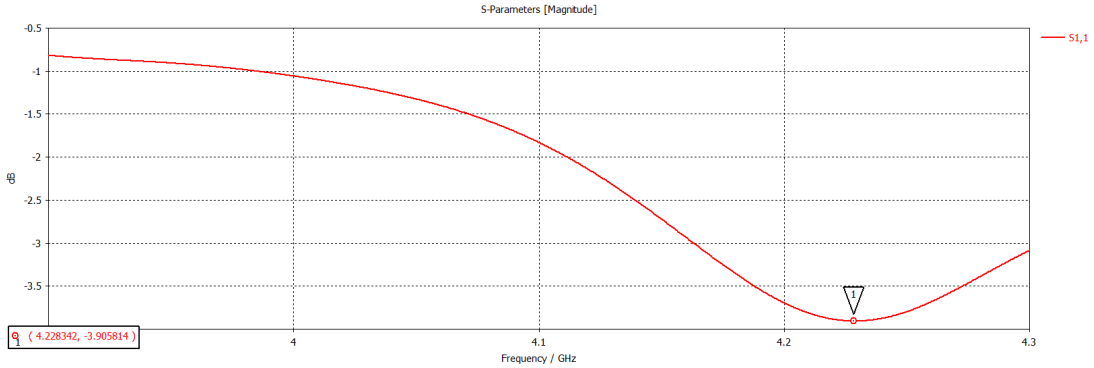

Model 5:

Top-view	Cross-section
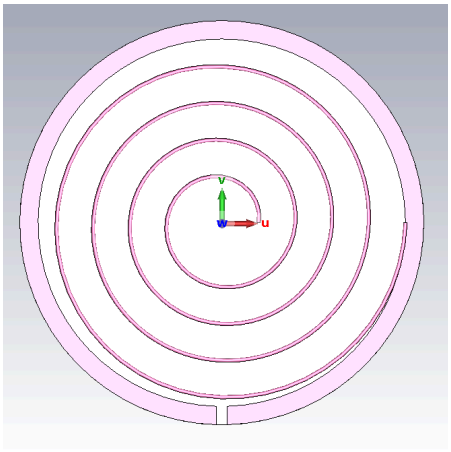	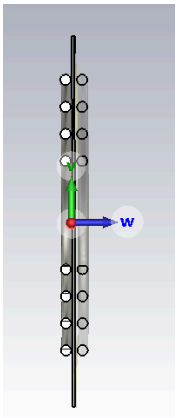

Resonance frequency:

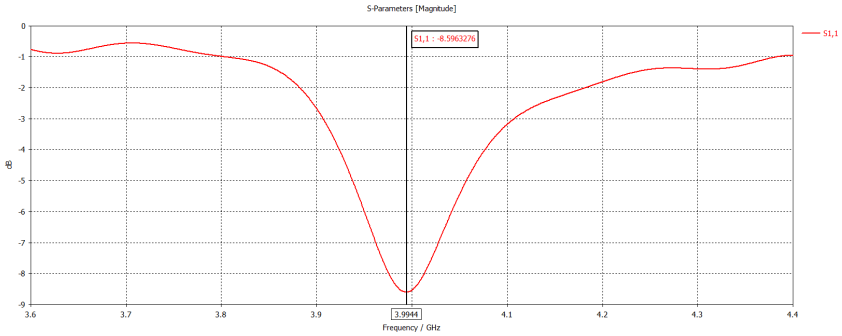

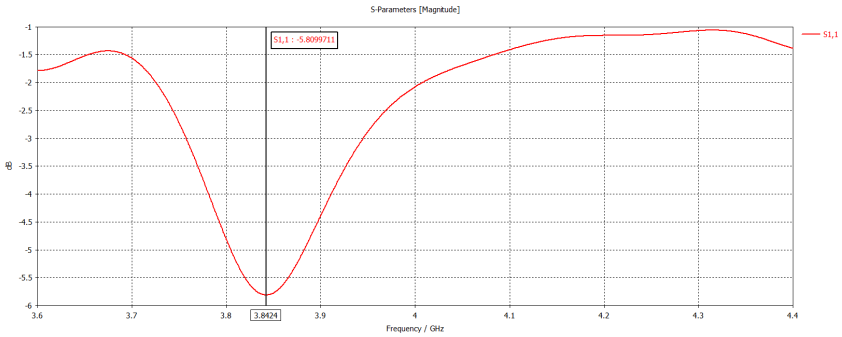

Model 6:

Top-view	Cross-section
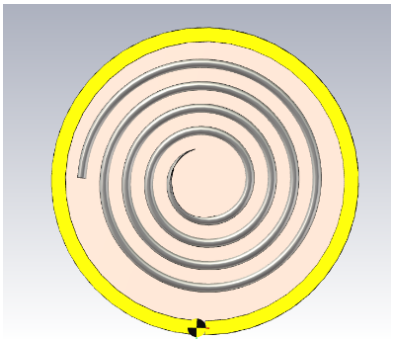	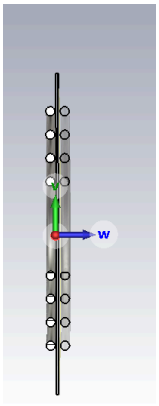

Resonance frequency:

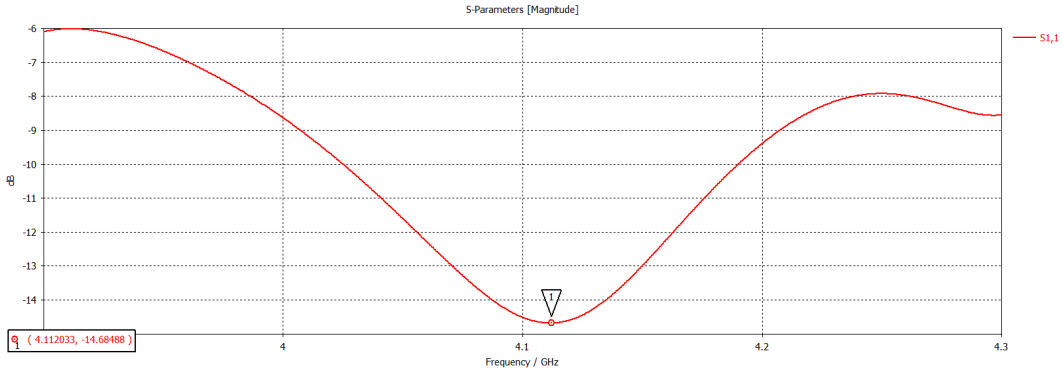

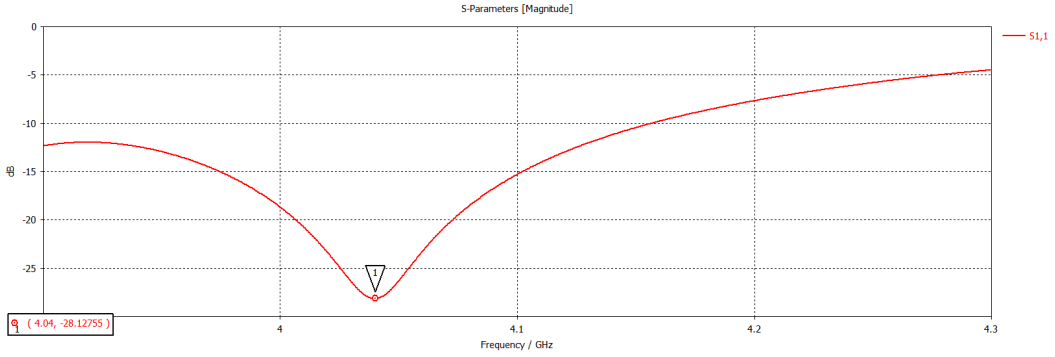

Model 7:

Top-view	Cross-section
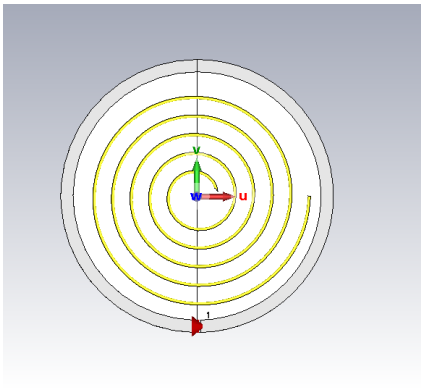	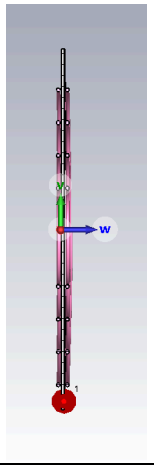

Resonance frequency:

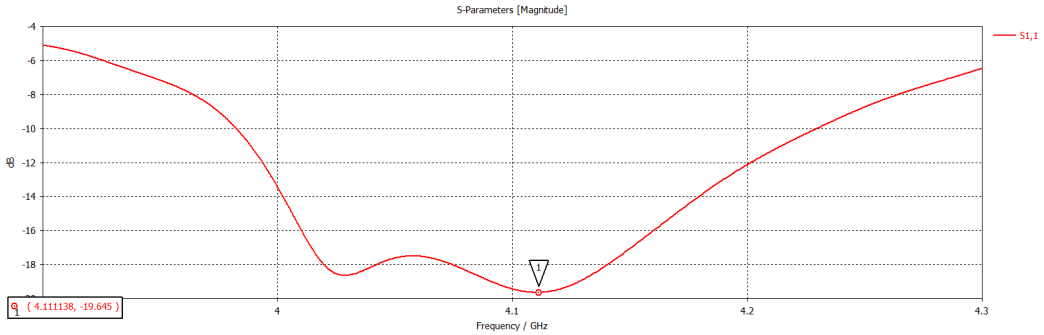

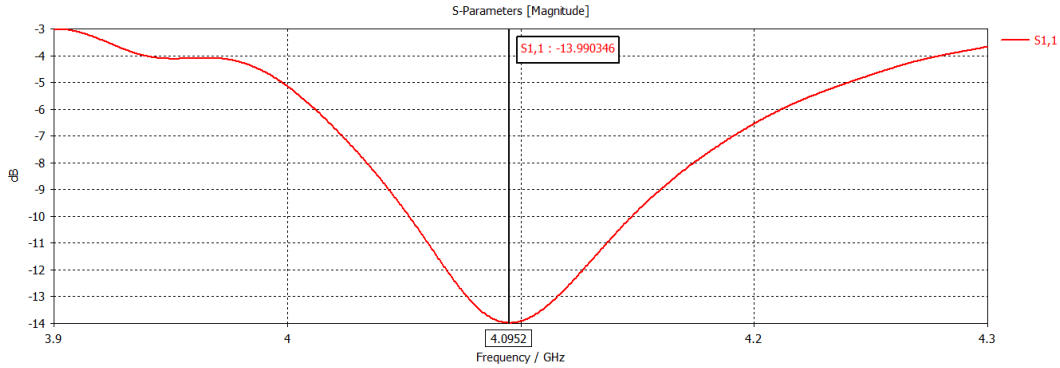

Model 8:

Top-view	Cross-section
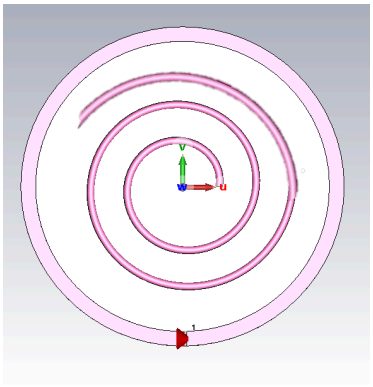	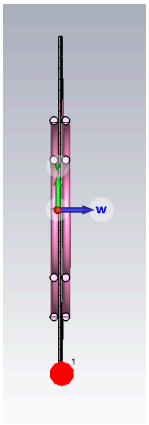

Resonance frequency:

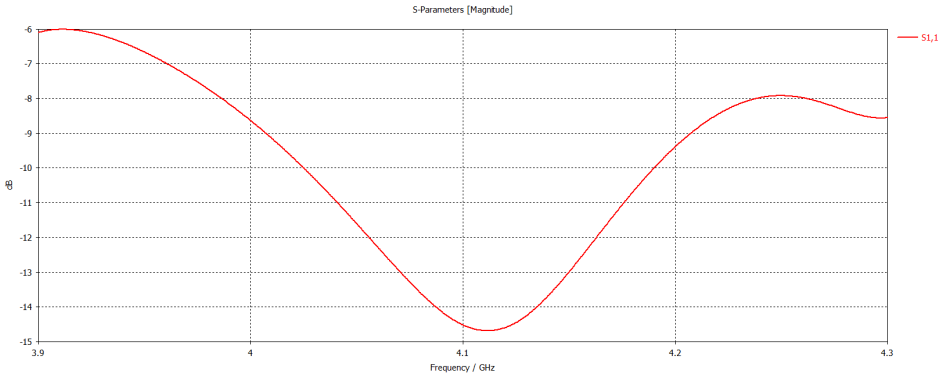

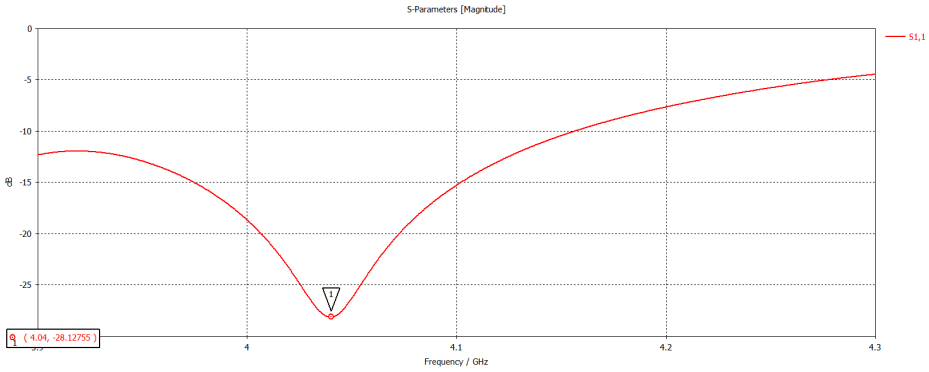

Model 9:

Top-view	Cross-section
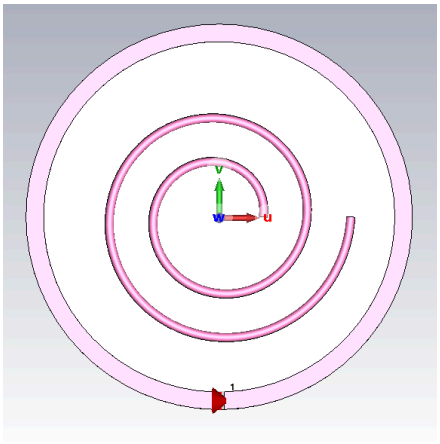	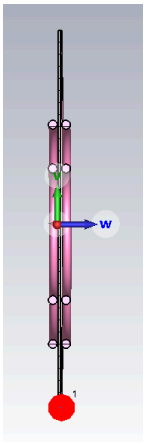

Resonance frequency:

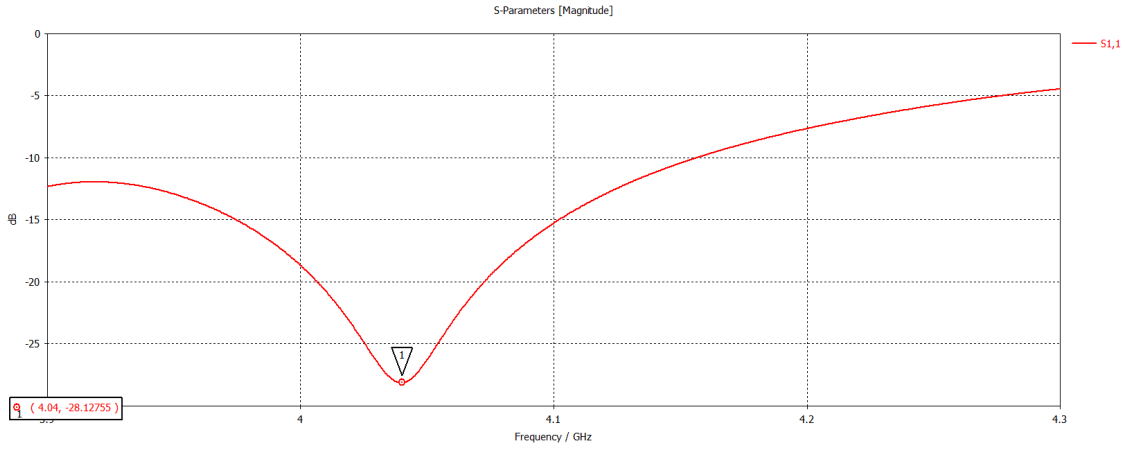

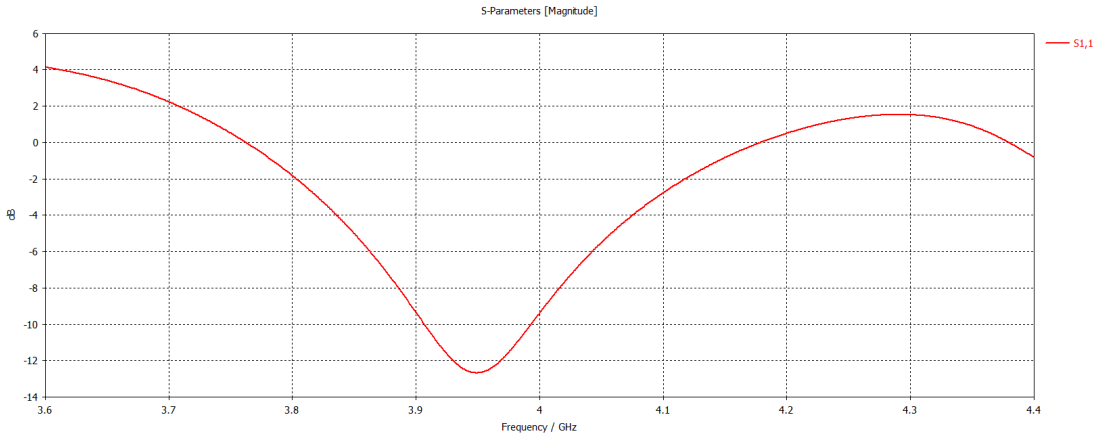

Model 11: 52

Top-view	Cross-section
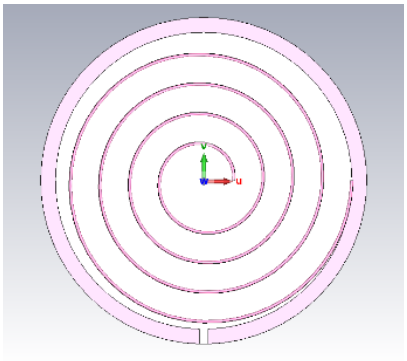	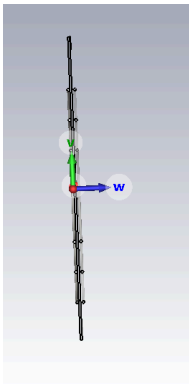

Resonance frequency:

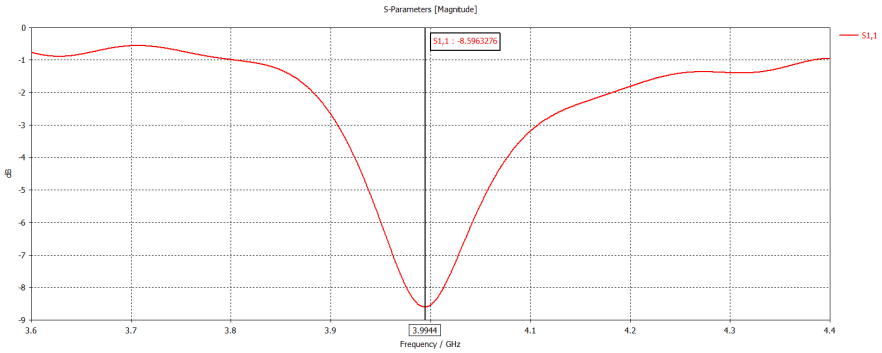

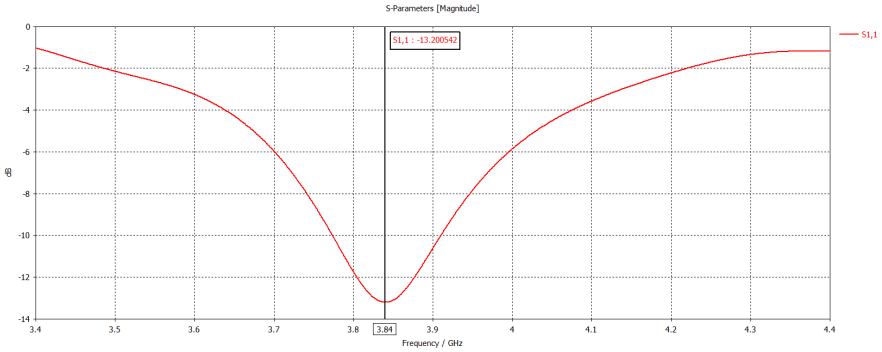

Model 12: 53

Top-view	Cross-section
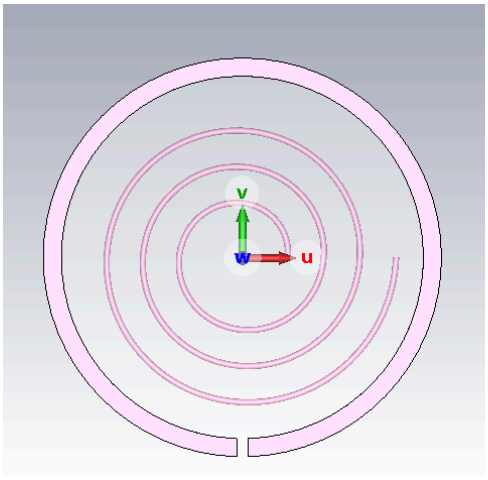	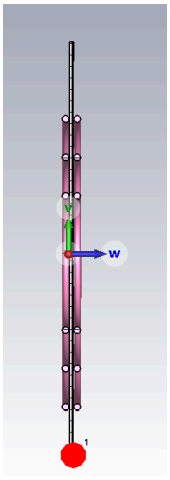

Resonance frequency:

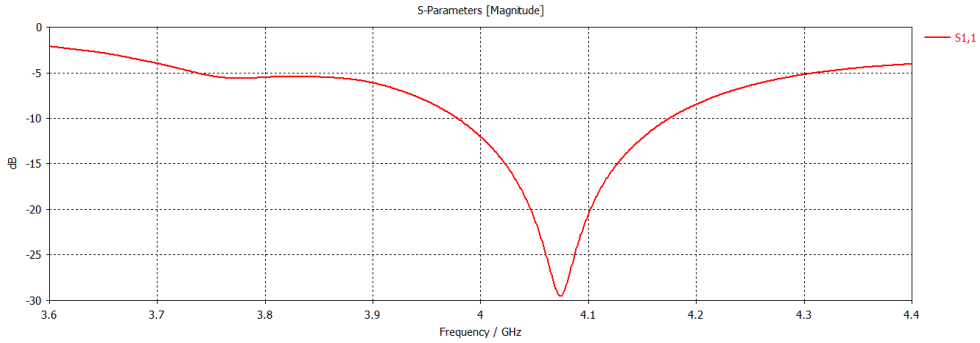

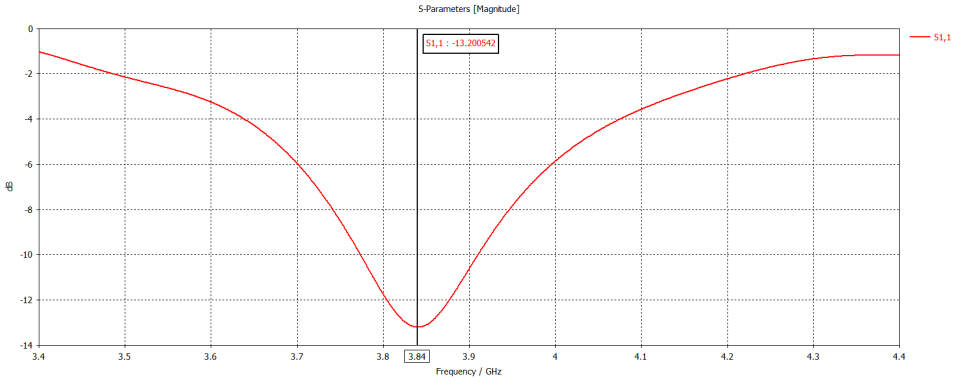

Model 13: 54

Top-view	Cross-section
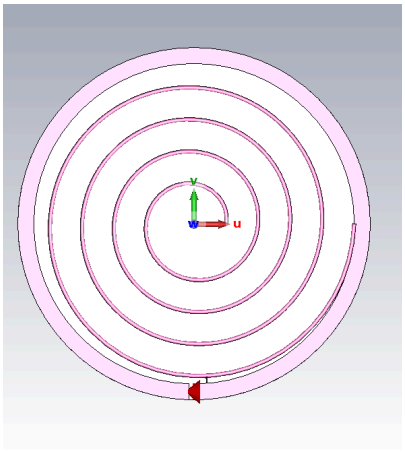	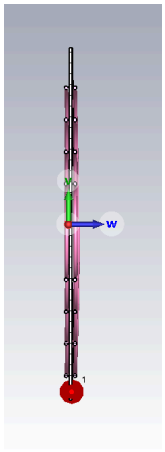

Resonance frequency: